



Holocene and Eemian climatic optima in the Korean Peninsula based on textural and carbon isotopic records from the stalagmite of the Daeya Cave, South Korea

Kyoung-nam Jo^a, Kyung Sik Woo^{b,*}, Hyoun Soo Lim^a, Hai Cheng^{c,d}, R. Lawrence Edwards^d,
Yongjin Wang^e, Xiuyang Jiang^e, Ryeon Kim^b, Jae Il Lee^a, Ho Il Yoon^a, Kyu-Cheul Yoo^a

^a Korea Polar Research Institute, KORDI, Incheon 406-840, Republic of Korea

^b Department of Geology, Kangwon National University, Gangwondo 200-701, Republic of Korea

^c Institute of Global Environmental Change, Xi'an Jiaotong University, Xi'an, Shaanxi 710049, China

^d Department of Geology and Geophysics, University of Minnesota, MN 55455, USA

^e Department of Geography, Nanjing Normal University, Nanjing, China

ARTICLE INFO

Article history:

Received 21 September 2010

Received in revised form

12 February 2011

Accepted 28 February 2011

Available online 21 March 2011

Keywords:

Stalagmite

Climatic optimum

East Asian monsoon

Palaeoclimate

Stable isotopes

ABSTRACT

Textural and stable isotopic records from the absolute-dated stalagmite of the Daeya Cave (DY-1) provide new insights into the climatic evolution of the Korean Peninsula during the Holocene and Eemian climatic optima. The stalagmite yielded ages of 8572 ± 227 to 5907 ± 158 and $1,23,456 \pm 535$ to $1,19,837 \pm 1089$ years, which coincide with the Holocene and Eemian climatic optima, respectively. The stalagmite's $\delta^{13}\text{C}$ record closely resembles previously reported Chinese speleothem $\delta^{18}\text{O}$ data. Thus it can be suggested that textural and geochemical results of the DY-1 reflect East Asian monsoon intensity, which is forced by summer insolation patterns in the northern hemisphere. Lighter carbon isotopic compositions, well-developed fibrous calcite crystals, and their relatively faster growth rate in the stalagmite sample are interpreted to reflect the warmest and wettest climate conditions of the Holocene and Eemian interglacials. Both climatic optima took place when insolation was decreasing from its maximum level, temperature in Greenland was highest, and sea level approached its maximum level. These climatic optima also coincide with decreasing Antarctic temperatures. Compared the DY-1 data to other proxies, it is suggested that the Holocene and Eemian climatic optima developed through a balance among boreal insolation, monsoon intensity, and sea level (also continental ice volume), which are the main climatic forcing factors in the northern hemisphere. These trends also follow the bi-polar seesaw mechanism as previously described.

© 2011 Elsevier Ltd. All rights reserved.

1. Introduction

Recent, rapid global warming will cause significant environmental changes and will make tremendous influence on socio-economic consequences (IPCC, 2007). Thus, it has been a key issue to predict future climate changes properly. In this respect, previous intervals of global climate warming have been considered to be ideal counterparts to understand present-day abrupt climate changes. Palaeoclimate records for the climatic optima of the current and previous interglacials may provide valuable information to help predict future climate conditions and environmental responses, as well as a good opportunity to test natural climate dynamics.

Early to middle Holocene and most of Eemian interval have been regarded as one of the warmest periods in the late Quaternary glacial-interglacial cycles, and temperatures during those times were similar to or possibly warmer than those of the present (e.g., An et al., 2000; Kukla et al., 2002). Numerous studies have focused on these two time intervals (e.g., An et al., 2000; Zhou et al., 2004; Oppo et al., 2006). The Holocene climatic optimum (HCO; hypsithermal or altilthermal) corresponds to a time of consistent high-summer insolation in the northern hemisphere, with the North American ice sheet no longer large enough to influence climate at a hemispheric scale (Wanner et al., 2008). Timing and duration of the HCO have been described for numerous regions worldwide. Although this relatively warm, wet interval lasted from about 9 to 6–5 ka (e.g., Wanner et al., 2008), results from previous studies of China are still controversial (An et al., 2000; Cai et al., 2010a), and the exact causes for the evolution of the HCO remain unclear. Despite numerous reports on palaeoclimatic studies during the Eemian period, the Eemian

* Corresponding author. Tel.: +82 33 250 8556; fax: +82 33 244 8556.

E-mail address: wooks@kangwon.ac.kr (K.S. Woo).

climatic optimum (ECO) has been documented in only a few regions and its palaeoclimatic implications remain still controversial, probably because of different sensitivities of climate proxies and/or a lack of reliable age-determination methods. Also, it may be because there are two different entities as follows: vegetation-defined Eemian interglacial and marine isotope stage (MIS) 5e from benthic foraminiferal $\delta^{18}\text{O}$ records. Shackleton et al. (2003) suggested that the timing of Eemian interglacial and MIS 5e could be different based on marine and continental records from the MD95-2042 core taken in southern Portugal. This indicates that different climatic components might show different phase relationship with respect to climate forcing. Various proxy data have shown different ages for ECO. For example, an interval of rapid speleothem deposition between 122 and 116 ka indicates fully interglacial conditions at an Austrian high alpine site (Spötl et al., 2002). According to Oppo et al. (2006), the ECO in the subpolar North Atlantic region peaked at approximately 125 ka and lasted $\sim 2\text{--}3$ k.y. Pollen records from Europe indicate that the ECO occurred at ~ 125 ka (Tzedakis, 2007). In contrast, stalagmite data from Italy suggest that optimal interglacial conditions were reached by ~ 129 ka and lasted ~ 2 k.y. (Drysdales et al., 2005).

A detailed understanding of the HCO and ECO requires high-resolution climate-sensitive proxies and precise age-dating methods because each of these climatic optima developed gradually, as compared to the more abrupt records of glacial-interglacial or stadial-interstadial changes. Speleothems have offered great potential for such detailed investigations (e.g., Fleitmann and Spötl, 2008) and have been regarded as a suitable material for palaeoclimatic reconstructions in regions affected by the Asian monsoon. Numerous speleothem studies have examined millennial- to orbital-scale evolution of the East Asian monsoon, which can cause severe droughts or floods over large, densely populated regions (e.g., Wang et al., 2001, 2005b, 2008; Cosford et al., 2008, 2010). Especially, high-resolution oxygen isotope records from Dongge and Sanbao caves in China showed continuous and detailed records of East Asian summer monsoon variations. It was suggested that Holocene and Eemian interglacial peaks which may well represent higher precipitation occurred at about 10–6 ka and 126–122 ka, respectively (Yuan et al., 2004; Wang et al., 2008). These studies, however, did not focus on the HCO and ECO. Furthermore, although speleothem-derived palaeoclimatic information from central to southern mainland China is abundant, speleothem records are lacking from the coastal regions of Far East Asia, including Korea and Japan (Jo et al., 2010a). Korean peninsula, located in the northeastern part of Asia, has been also affected by East Asian monsoon climate. However, due to its geographic setting the peninsula has also been affected by ocean climate system which are intimately related to eustatic sea-level changes and corresponding palaeo-current systems. Thus, speleothem records in the peninsula should provide clues to re-interpret the causes of climate optimum which has been explained by insolation-induced East Asian monsoonal changes. This study will help to understand palaeoclimatic evolution and its mechanisms of the regions affected by various climate controlling factors.

This paper presents a well-defined stalagmite record that provides a perspective on HCO and ECO evolution on the Korean Peninsula. A composite-type speleothem record from the eastern part of the Korean Peninsula (Jo et al., 2010a) demonstrated that variations in $\delta^{13}\text{C}$ values and corresponding textural changes can be used as palaeoclimatic proxies, instead of more widely used $\delta^{18}\text{O}$ record. The present study focuses on $\delta^{13}\text{C}$ variations and growth patterns, including crystal texture and growth intervals, to reconfirm previous results and address the palaeoclimatic evolution of Far East Asia during the HCO and ECO.

2. Geographic setting

The Korean Peninsula is on the margin of north-eastern Asia (Fig. 1A, B), a region that has been strongly affected by the East Asian monsoonal climate for several million years (Wang et al., 2005a). The climate of the Korean Peninsula is warm and humid in summer and cold and dry in winter, with a 30-year mean annual precipitation of 1402 mm. 75% of the annual precipitation takes place during summer rainy season. The mean annual temperature is 12.9 °C, with a winter minimum of -6.5 °C (January) and a summer maximum of 25 °C (August; Korea Meteorological Administration; <http://www.kma.go.kr>).

Every year, monsoon rain first appears in May in southern China (An et al., 2000). By July the rain has moved north into Japan and the Korean Peninsula. Major air masses that influence the climate of the Korean Peninsula are the northern Pacific air mass (NP), Siberian air mass (S), Yangtze River air mass (YR), and Okhotsk Sea air mass (OS; Fig. 1B). When both Siberian and North Pacific high-pressure cells are weak in spring and autumn, the Yangtze River and Okhotsk Sea air masses control the climate of Korea. In early summer, a heavy rainfall front (called 'jang-ma' in Korean) passes northward through the Korean Peninsula along the contact between the Okhotsk Sea and Northern Pacific air masses. Winds blowing from west to east high at mid-altitude also contribute to Korean climate conditions. The subpolar front, a thermal boundary between warm southern and cold northern water masses, forms near 37°N, where the cold water mass separates from the eastern coast of the Korean Peninsula (Lee, 2007; Fig. 1B). The Korean Peninsula is also affected by typhoons between June and September.

This study analyzed a damaged speleothem (stalagmite) sample collected from Daeya Cave (Yeongweol-gun, Gangwon-do), located in the central part of the Korean Peninsula. Daeya Cave is in the Ordovician Maggol and Duwibong formations of the Taebaek Group, Joseon Supergroup (Fig. 1B). These formations are dominated by limestone to argillaceous limestone, with sparse dolostone layers, and represent shallow marine and tidal environments (Woo and Park, 1989). The strata were tectonically uplifted and fractured during the development of large NE- to NNE-trending thrusts during the Jurassic (Chough et al., 2000), resulting in numerous faults and joints along which cave development took place (Fig. 1B and supplementary data). The land surface now consists of a steep slope covered with dense vegetation. The entrance of Daeya Cave is 190 m above sea level, and the total length of the cave is about 450 m. The cave temperature is roughly uniform throughout the year, ranging from 13.3 to 14.5 °C (supplementary data). The annual average humidity is almost 100%. Daeya Cave is a relatively deep cave that is more than 200 m below the land surface, except for the entrance area.

3. Material and methods

An 11.5 cm-long broken stalagmite sample (DY-1) was collected about 250 m from the entrance of Daeya Cave (Fig. 2 and supplementary data). Stalagmite DY-1 is a typical bell-shaped stalagmite consisting of translucent, yellowish, densely packed calcite crystals with minor, relatively porous, opaque, yellowish to white calcite (Fig. 2).

The stalagmite sample was cut into two pieces along the growth axis. Thin sections were made from one half and were examined with a polarizing microscope for textural description. Acetate peels were prepared from the other half to supplement the thin-section examination. After textural examination, thin sections were stained with Feigl's solution in order to distinguish aragonite from calcite. The mineralogy of DY-1 was confirmed using X-ray diffraction (XRD; Rigaku, JP/D/MAX-2200H) at Kangwon National University (Republic of Korea).

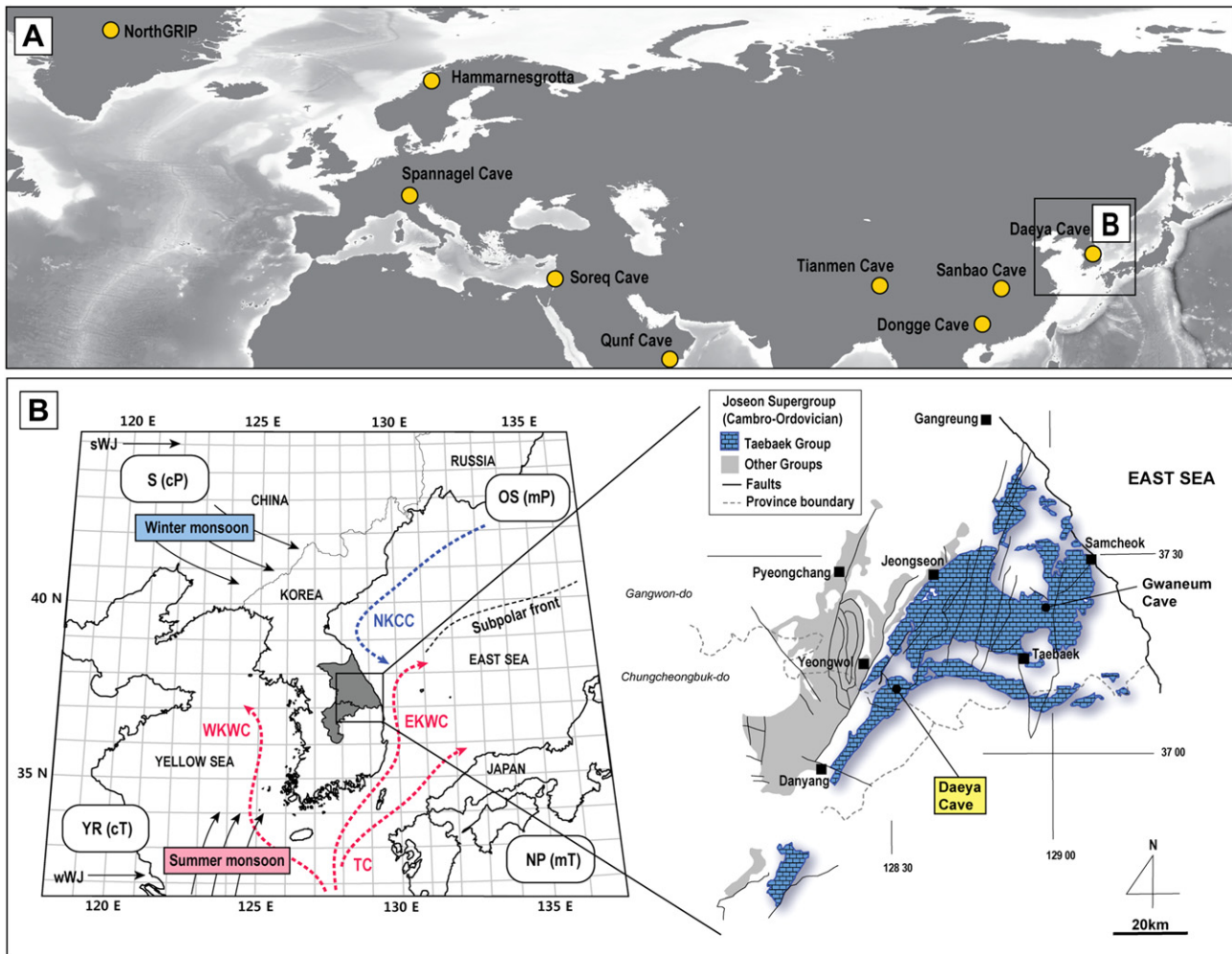


Fig. 1. (A) Location of Daeya Cave as well as other caves mentioned in the text, and the NGRIP ice-core site. (B) Atmospheric and oceanographic settings around the Korean Peninsula (left panel) and geologic setting with the locality of Daeya Cave (right panel). S = Siberian air mass, OS = Okhotsk Sea air mass, NP = Northern Pacific air mass, YR = Yangtze River air mass, sWJ = summer westerly jet, wWJ = winter westerly jet, TC = Tsushima current, WKWC = West Korean warm current, EKWC = East Korean warm current, NKCC = North Korean cold current.

The depositional age of DY-1 is based on 10^{234}U – ^{230}Th dates measured at the University of Minnesota (USA), using conventional chemical separation and inductively coupled plasma mass spectrometry (ICP-MS; Finnigan-MAT Element; Fig. 2). All reported ratios are activity ratios with 2σ errors. All ^{230}Th dates of the subsamples considered here are in correct stratigraphic order within error.

For $\delta^{18}\text{O}$ and $\delta^{13}\text{C}$ analyses, approximately $100\ \mu\text{g}$ of powder were drilled using a $0.3\ \text{mm}$ diameter drill bit at $0.5\ \text{mm}$ intervals along the stalagmite's growth axis (212 samples; Fig. 2), and analyzed using a Finnigan MAT-253 ratio mass spectrometer with an on-line, automated, carbonate preparation system (Kiel III) at Nanjing Normal University, China. Measured C- and O-isotope ratios are reported in the per mil (‰) notation relative to the PDB standard. Analytical errors for $\delta^{18}\text{O}$ and $\delta^{13}\text{C}$ are 0.15 and 0.2‰ , respectively.

4. Results

4.1. Texture

The distinctive physical features of the stalagmite DY-1 are a thin, porous, white growth phase between two dense, translucent

yellowish phases (Fig. 2). Based on these textural characteristics, DY-1 has three growth phases (phases A, B, and C) with boundaries at 88 and 93 mm from the base; the lengths of the three growth phases are 88, 5, and 12 mm, respectively.

Phase A is a typical, bell-shaped stalagmite that is thicker in diameter toward its base. Although Phase A consists entirely of translucent, yellowish, low-Mg calcite and appears to lack distinctive growth laminae, the acetate peel reveals numerous micron-scale growth laminae (Fig. 3A), reflecting high-frequency cyclic changes probably created by the change of cave drip-water contents during its growth. Such bands are thicker in the lower part of Phase A than in its upper part (Fig. 3A), probably implying the change of relative growth rate. The morphology of Phase A calcite crystals is fibrous to highly elongated columnar calcite (length to width ratio: $\geq 6:1$; e.g., Frisia et al., 2000 and references cited therein), with straight crystal and sub-crystal boundaries (Fig. 3B). There is no petrographic evidence of any significant depositional hiatus in Phase A.

Textural difference between phases A and B is very clear (Figs. 2, 3B and 3C). Phase B is much more sparse than Phase A. The boundary between Phase A and Phase B is characterized by the sharp termination of columnar calcite crystals of Phase A and the initiation of new crystallites, indicating that there was a hiatus

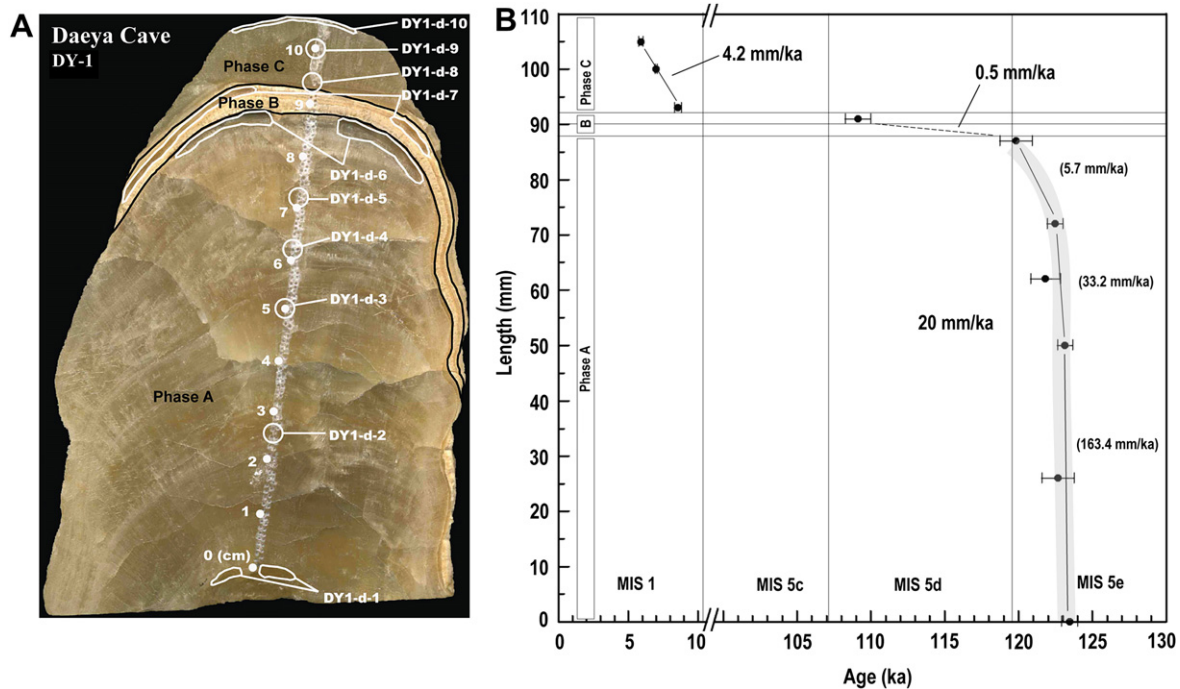


Fig. 2. (A) A slab of stalagmite DY-1 showing sub-sampling sites for carbon and oxygen isotope analysis and uranium-series dating. Growth phases are texturally divided into phases A, B and C. (B) ^{230}Th ages along the growth axis (right panel). Solid and dashed lines that connect the dates show age model for DY-1. The gray zone in Phase A indicates the most probable age range. Estimated growth rate and marine isotope stages (MIS) are also indicated.

between precipitation of the two growth phases (lower white arrow in Fig. 3C). Most of Phase B consists of much smaller and commonly fibrous calcite (2 mm long, 0.1–0.5 mm thick) with serrate crystal boundaries and more abundant growth laminae than those of Phase A. Phase B can be divided into lower and upper parts on the basis of textural differences in the calcite crystals (Fig. 3C). The lower part is characterized by extremely dense, dark growth laminae consisting predominantly of obscure fibrous calcite with micritic calcite (similar to tufa fabric described by Frisia et al., 2000). The c-axes of these fibrous calcite crystals are commonly truncated. The upper part of Phase B consists of relatively well-developed fibrous to elongated columnar calcite with serrate crystal boundaries. Fibrous to elongated columnar crystals in this part are not optically continuous with those of lower Phase B, indicating another significant hiatus (middle white arrow in Fig. 3C). The uppermost part of Phase B, near the boundary with Phase C, consists of extremely dark, dense growth laminae (Fig. 3C).

Crystal morphology of Phase C strongly resembles that of Phase A (Fig. 3B, D). Crystallites of the fibrous to elongated columnar calcite in this growth phase nucleated on the boundary between phases B and C, marking another, probably lengthy interruption in growth (upper arrow in Fig. 3C).

4.2. U-series dating

Concentrations of U in DY-1 range from 70.6 to 167.7 ppb (Table 1). The samples do not contain sufficient ^{232}Th contamination to affect the age determinations, and all dates for DY-1 are in stratigraphic order within 2σ error. The 2σ errors for all dates range from 0.4 to 2.9% and are typically around 0.5% for the older part of the speleothem. The oldest ^{230}Th age for DY-1, obtained from the base of the stalagmite, is $1,23,456 \pm 535$ years, and the youngest age, from the uppermost part, is 5907 ± 158 years (Fig. 2). The two brief growth intervals represented by phases A and C correspond to less than 10% of the total age span of the speleothem. On the basis

of ^{230}Th dating results, Phase A grew from $1,23,456 \pm 535$ to $1,19,837 \pm 1089$ years ago, with a mean growth rate of about 20 mm/ka (Table 1; Fig. 2). Phase B formed predominantly before $1,09,134 \pm 863$ years ago, the age of the upper part of the growth phase. Phase C formed from 8572 ± 227 to 5907 ± 158 years ago, with a mean growth rate of 4.2 mm/ka.

4.3. Stable isotopes

High-resolution stable isotope profiles were obtained for DY-1 to understand and compile the continuous palaeoclimatic record (Fig. 4A). The $\delta^{18}\text{O}$ values for the entire record of DY-1 range from -9.2 to -7.4 ‰, with an average of 8.6 ‰. The corresponding $\delta^{13}\text{C}$ values range from -9.7 to -3.6 ‰, with an average of -8.0 ‰. Carbon isotopic compositions vary considerably along the growth axis of the stalagmite, whereas oxygen isotope values are comparatively stable except for Phase B. The average values of both isotopes in each phase are distinctive, and the isotopic variations show distinct patterns at the boundaries between the growth phases.

The $\delta^{18}\text{O}$ values in Phase A range from -9.2 ‰ to -7.8 ‰, with an average value of -8.6 ‰ without distinctive patterns or anomalies (Fig. 4A). The $\delta^{13}\text{C}$ values for Phase A vary between -9.8 and -6.4 ‰, with an average value of -8.5 ‰. Although their variations outline irregular, high-frequency fluctuations, distinct positive anomalies with amplitudes of 1–2‰ are present at 11, 21, 35, 49, and 78 mm (Fig. 4A). The most obvious isotopic excursions are in uppermost Phase A, where the carbon isotope ratio increases by more than 4‰ and the oxygen isotope ratio increases by more than 1.5‰. In Phase B, the oxygen isotopic composition ranges from -8.8 to -7.4 ‰, and the carbon isotopic composition ranges from -5.7 to -3.7 ‰ (Fig. 4A). Average values of both isotopes in this phase are -8.1 and -4.6 ‰, respectively. Variations of $\delta^{18}\text{O}$ and $\delta^{13}\text{C}$ values in Phase B show similar patterns and amplitudes (up to ~ 1.4 ‰ for $\delta^{18}\text{O}$ and 2‰ for $\delta^{13}\text{C}$). Phase B initiated with $\delta^{18}\text{O}$ and $\delta^{13}\text{C}$ values of -7.4 and -3.7 ‰ followed by a steep trend towards lower values, and then

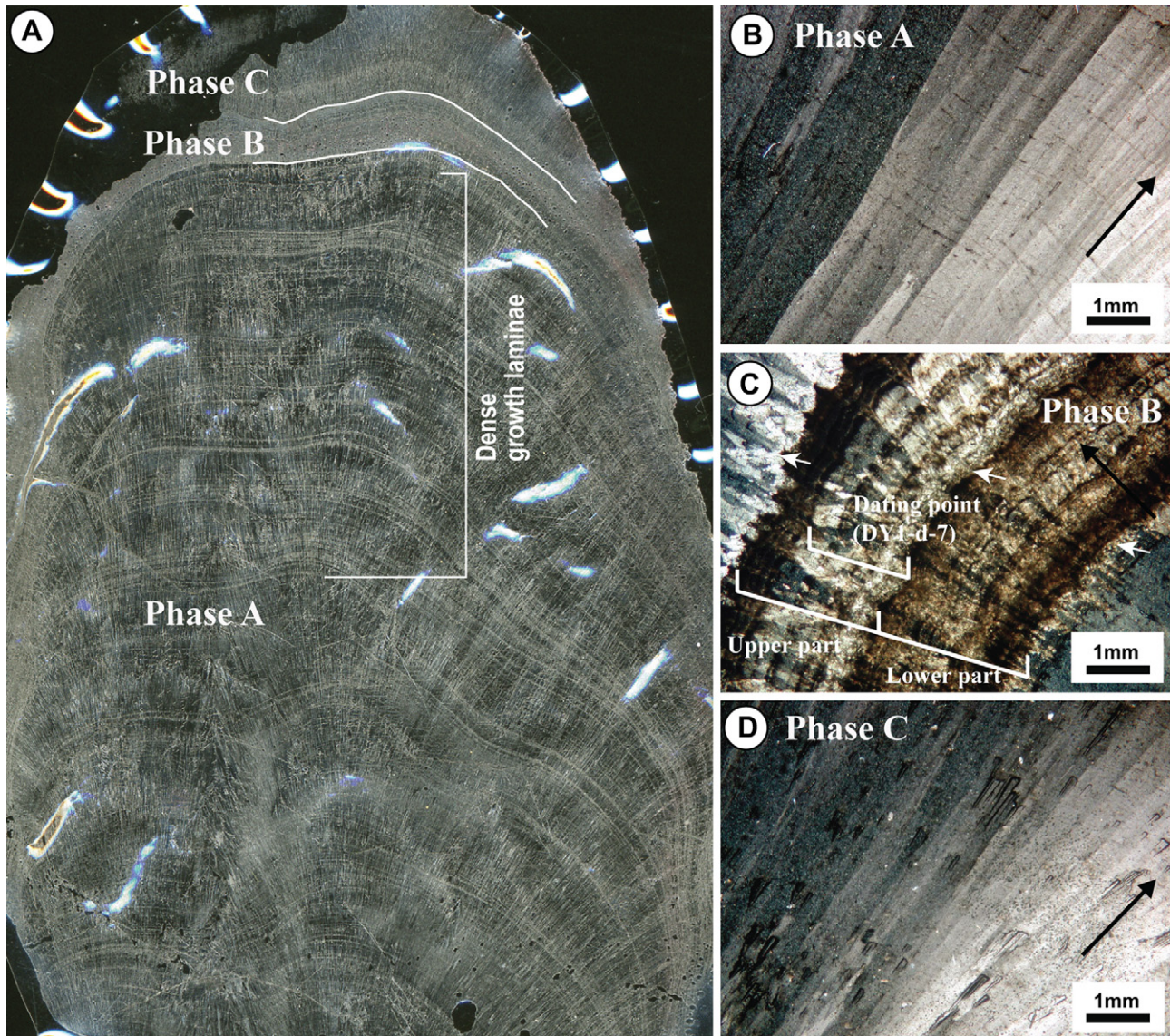


Fig. 3. Photomicrographs of an acetate peel (A) and thin sections (B–D; under cross-polarized light) of DY-1 showing calcite crystal textures. A) An acetate peel showing three distinct growth phases. Note more densely spaced growth laminae in the upper part of Phase A. B) Elongated columnar calcite with straight crystal and sub-crystal boundaries in Phase A. C) Fine, fibrous calcite crystals with serrated crystal boundaries in Phase B. Note that the growth of fibrous calcite was terminated at several stages, commonly interrupted by thick growth laminae. The area sampled for dating purposes is indicated (as dating point). D) Well-developed fibrous calcite crystals of Phase C. Growth directions (black arrows) and texturally observed hiatuses (small white arrows in C) are indicated.

a rapid increase. The $\delta^{18}\text{O}$ values of Phase C fluctuate between -9.2 and -7.7‰ , with an average value of -8.6‰ . Phase C $\delta^{13}\text{C}$ values range from -6.7 to -4.6‰ , with an average value of -6.1‰ . Stable isotopic variations of Phase C are characterized by abrupt depletion of ^{18}O and ^{13}C in the lowermost part of the growth phase, followed by a gradual decrease in $\delta^{18}\text{O}$ values and relatively stable $\delta^{13}\text{C}$ values.

A scatter diagram of $\delta^{18}\text{O}$ and $\delta^{13}\text{C}$ values shows different ranges for each growth phase (Fig. 4B); these distinctive domains are largely a function of carbon isotopic composition. A strong correlation exists between $\delta^{18}\text{O}$ and $\delta^{13}\text{C}$ values of Phase B, whereas phases A and C lack covariance in ^{18}O and ^{13}C except at phase boundaries.

5. Data interpretation

5.1. Age model

A detailed age model for stalagmite DY-1 was derived by linear interpolation between all dates except for DY1-d-2 and -d-4, which

are slightly out of stratigraphic order even though they are within 2σ error (Table 1; Fig. 2). The growth pattern of DY-1 is characterized by two short intervals of rapid growth separated by a long-term hiatus (approximately 1,01,000 years) between phases B and C (supplementary data).

Although the age of the base of the stalagmite cannot be determined due to the previous use for age dating that did not provide reliable results, it can be assumed that Phase A started to grow just before 123.5 ka because the lower part of Phase A has the fastest growth rate (163.4 mm/ka) of the entire sample and the age of the lowermost part can be extrapolated from the uniform growth rate during this interval (Fig. 2). Based on the ages from its bottom to the top, Phase A formed from 123.5 to 119.8 ka (a time interval of 3.7 k.y.). Although the mean growth rate of Phase A can be calculated as 20 mm/k.y. by assuming a constant growth rate, it is more plausible that the growth rate gradually decreased from 163.4 to 5.7 mm/k.y. toward the upper part of Phase A (Fig. 2). This is supported by the greater density of growth bands in the upper

Table 1²³⁰Th dating results of the DY-1 stalagmite. The error is 2 σ error. Bold values indicate final corrected ages indicated in Fig. 2B.

Sample number	²³⁸ U (ppb)	²³² Th (ppt)	²³⁰ Th/ ²³² Th (atomic $\times 10^{-6}$)	²³⁴ U ^a (measured)	²³⁰ Th/ ²³⁸ U (activity)	²³⁰ Th Age (yr) (uncorrected)	²³⁰ Th Age (yr) (corrected)	²³⁴ U ^{initial} ^b (corrected)
DY1-d-1	135.7 \pm 0.2	371 \pm 19	9807 \pm 505	1207 \pm 3	1.6260 \pm 0.004	1,23,542 \pm 535	1,23,456 \pm 535	1711 \pm 4
DY1-d-2	139.6 \pm 0.4	230 \pm 565	16418 \pm 204	1237 \pm 6	1.6411 \pm 0.024	1,22,692 \pm 1102	1,22,675 \pm 1,102	1749 \pm 15
DY1-d-3	111.2 \pm 0.2	185 \pm 20	16590 \pm 1761	1268 \pm 3	1.6711 \pm 0.004	1,23,225 \pm 501	1,23,150 \pm 501	1796 \pm 4
DY1-d-4	127.1 \pm 0.3	579 \pm 206	6204 \pm 122	1337 \pm 7	1.7127 \pm 0.024	1,21,873 \pm 1009	1,21,827 \pm 1,009	1887 \pm 12
DY1-d-5	128.0 \pm 0.2	269 \pm 20	13423 \pm 986	1324 \pm 3	1.7088 \pm 0.004	1,22,567 \pm 523	1,22,488 \pm 523	1870 \pm 5
DY1-d-6	130.8 \pm 0.3	6135 \pm 113	610 \pm 1	601 \pm 8	1.7325 \pm 0.008	1,20,302 \pm 1069	1,19,837 \pm 1,089	1937 \pm 9
DY1-d-7	167.7 \pm 0.3	13667 \pm 37	338 \pm 2	1422 \pm 4	1.66585 \pm 0.007	1,09,945 \pm 767	1,09,134 \pm 863	1935 \pm 7
DY1-d-8	80.1 \pm 0.1	2352 \pm 47	120 \pm 3	1703 \pm 3	0.2145 \pm 0.001	8942 \pm 55	8572 \pm 227	1745 \pm 3
DY1-d-9	70.6 \pm 0.1	469 \pm 18	423 \pm 16	1679 \pm 3	0.1705 \pm 0.001	7122 \pm 36	6994 \pm 62	1713 \pm 3
DY1-d-10	133.8 \pm 0.2	3355 \pm 14	95 \pm 1	1615 \pm 4	0.14474 \pm 0.002	6183 \pm 76	5907 \pm 158	1642 \pm 4

 $\lambda_{230} = 9.1577 \times 10^{-6} \text{ y}^{-1}$, $\lambda_{234} = 2.8263 \times 10^{-6} \text{ y}^{-1}$, $\lambda_{238} = 1.55125 \times 10^{-10} \text{ y}^{-1}$.Corrected ²³⁰Th ages assume the initial ²³⁰Th/²³²Th atomic ratio of $4.4 \pm 2.2 \times 10^{-6}$. Those are the values for a material at secular equilibrium, with the bulk earth ²³²Th/²³⁸U value of 3.8. The errors are arbitrarily assumed to be 50%.^a $\delta^{234}\text{U} = ([^{234}\text{U}/^{238}\text{U}]_{\text{activity}} - 1) \times 1000$.^b $\delta^{234}\text{U}_{\text{initial}}$ was calculated based on ²³⁰Th age (T), i.e., $\delta^{234}\text{U}_{\text{initial}} = \delta^{234}\text{U}_{\text{measured}} \times e^{\lambda_{234} \times T}$.

part of Phase A relative to the lower part (Fig. 3A). Phase A grew during the peak of the Last Interglacial [Marine Isotope Stage (MIS) 5e], and the timing of the first growth hiatus of DY-1 corresponds to the inception of the last glacial (MIS 5d; Martinson et al., 1987; Fig. 2). Thus, Phase A grew continuously during late MIS 5e, with a gradually decreasing growth rate. Although there is only one date for Phase B, owing to difficulty in sub-sampling this very thin growth phase, the upper part of the phase yielded an age of 109.1 ka (Table 1). This result clearly indicates that the brief growth interval of Phase B, which is composed of small, porous, sparse fibrous calcite crystals with several hiatuses, was formed at some time during the MIS 5d stadial (Fig. 2). Assuming continuous growth, the mean growth rate of Phase B can be estimated as 0.5 mm/k.y., but numerous textural discontinuities in Phase B suggest that its growth was, in fact, intermittent (Fig. 3C). Even though Phase B formed during a very short interval within MIS 5d, a constant growth rate cannot be inferred, and a model age cannot be established due to these intermittent growth patterns as shown by textural characteristics. In contrast, three dates from Phase C, together with textural information, clearly indicate that it grew from 8.6 to 5.9 ka at a nearly constant growth rate of 4.2 mm/k.y. (Fig. 2). As a consequence, the age model for DY-1 is well constrained, except for Phase B. That is, growth of stalagmite DY-1 took place predominantly in two brief intervals: about 123.5–119.8 ka in late MIS 5e and 8.6–5.9 ka in early to middle MIS 1, with minor contributions during MIS 5d.

5.2. Isotopic equilibrium versus non-equilibrium deposition

In order to use stable isotopic records in interpreting palaeoclimate, it is necessary to establish that the speleothem precipitated under isotopic equilibrium conditions (e.g., Hendy, 1971; Dorale and Liu, 2009). However, there is as yet no accepted method of doing so. Several criteria for the identification of equilibrium deposition have been suggested. Of these methods, the Hendy Test, is the best known and most widely used (e.g., Zhou et al., 2008; Boch et al., 2009). The Hendy Test is based on three criteria: (1) invariability of oxygen isotope values along the same individual growth lines, (2) non-covariance of oxygen and carbon isotope values along individual layers, and (3) non-covariance of oxygen and carbon isotopic values along the growth axis. However, Dorale and Liu (2009) suggested that because a typical growth layer is generally thickest near the top surface of the stalagmite and becomes progressively thinner along the sides, a comparison of coeval sub-samples from the top to the sides is not truly valid, such that a negative result of the Hendy Test may not necessarily indicate kinetic fractionation or evaporation. This problem could be overcome by replication analyses, in which individual factors such as flow path, drip-water chemistry and temperature are separately ruled out.

Because stalagmite DY-1 has closely-spaced, dense laminae (Fig. 3A), microsampling along the same growth lamina is technically difficult. This means that testing the first and second

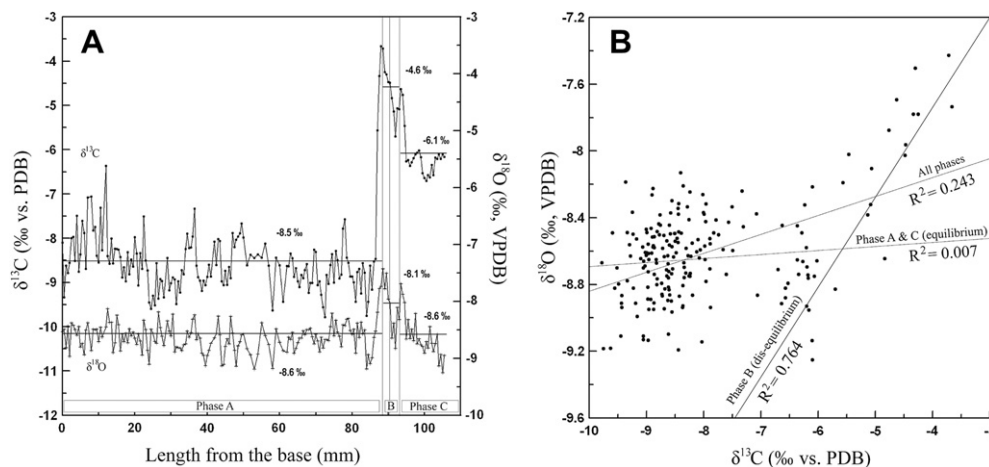


Fig. 4. Stable isotopic results from DY-1. A) A plot of $\delta^{18}\text{O}$ and $\delta^{13}\text{C}$ values versus distance from the base of the stalagmite. Vertical lines indicate locations of textural hiatuses. Note the five positive anomalies at 11, 29, 35, 49 and 78 mm above from the base. B) Scatter diagram of $\delta^{18}\text{O}$ versus $\delta^{13}\text{C}$ values for the three growth phases.

methods of the Hendy Test cannot be employed. A replication study was not performed because of the lack of other damaged stalagmites (cave conservation regulations prohibit collection of undamaged speleothems). In spite of these limitations, several other constraints confirmed that DY-1 formed under near-equilibrium conditions: (1) textural properties of the calcite crystals, (2) non-covariance along the growth axis (third component of the Hendy Test), and (3) strong similarities between the DY-1 $\delta^{13}\text{C}$ and $\delta^{18}\text{O}$ records and those from other Chinese caves. First, phases A and C have fibrous to columnar calcite crystal textures, indicating that the majority of the stalagmite probably precipitated under near-equilibrium isotopic conditions. Equivalence can be assumed because columnar and fibrous calcite develops only under constant discharge and low supersaturation of the parent waters (Frisia et al., 2000). Second, stable isotopic results for DY-1 (except Phase B) do not show systematic enrichment in ^{13}C and ^{18}O along the growth axis (Fig. 4B). This condition satisfies the third criterion of the Hendy Test: if CO_2 loss was rapid during growth of DY-1, kinetic fractionation would have occurred between HCO_3^- and $\text{CO}_{2(\text{aq})}$, and the isotopic results of stalagmite DY-1 would show a simultaneous enrichment in ^{13}C and ^{18}O along the growth axis (Hendy, 1971). Third, the DY-1 $\delta^{13}\text{C}$ pattern is very similar to Chinese cave $\delta^{18}\text{O}$ records at a millennial to sub-millennial scale during both the late Last Interglacial and early Holocene (Yuan et al., 2004; Wang et al., 2005b; Fig. 5), indicating that carbon isotope values of stalagmite DY-1 are dominated by regional palaeoenvironmental changes in East Asia rather than local effects in the individual caves and flow paths. This is also strongly supported by previous results showing that the stalagmite $\delta^{13}\text{C}$ record from the eastern Korean Peninsula is remarkably similar to Chinese cave $\delta^{18}\text{O}$ records during MIS 5a (Jo et al., 2010a). Together, this set of criteria indicates that phases A and C of DY-1 were deposited under isotopic equilibrium conditions, and confirms the palaeoenvironmental dependence of carbon isotope compositions in this speleothem.

5.3. Oxygen isotopes

Under isotopic equilibrium deposition, the oxygen isotope values of speleothems reflect cave temperature and oxygen isotopic composition of cave drip-water (Anderson and Arthur, 1983). These phenomena are controlled by the mean annual temperature and oxygen isotopic compositions of precipitation, respectively. The

oxygen isotope ratio of meteoric water is related to environmental factors such as the air temperature, source region, rainfall amount, and evaporation/vapour convergence ratio (e.g., Gascoyne et al., 1980; Fleitmann et al., 2003; Asmerom et al., 2007; Lee et al., 2009). In tropical and sub-tropical monsoon regions, including East Asia, speleothem $\delta^{18}\text{O}$ records show the influence of summer rainfall volume or seasonal precipitation (i.e., summer monsoon intensity). However, $\delta^{18}\text{O}$ values of modern precipitation in the Korean Peninsula do not reflect clear seasonal patterns (Yu et al., 2007; supplementary data), in contrast to the speleothem results in south-eastern China. This may imply that different atmospheric processes dominate the distribution of oxygen isotopes in the two regions. Furthermore, the oxygen isotopic results for DY-1 and for other speleothems from the Korean Peninsula do not evince any of the major climatic and environmental changes (Jo et al., 2010a, 2010b). Hence, $\delta^{18}\text{O}$ values from Korean speleothems are probably affected by unknown environmental factors that are distinct from controlling factors on speleothem $\delta^{18}\text{O}$ values in the tropical to sub-tropical Chinese mainland, despite both regions being strongly affected by the East Asian monsoon. Many issues related to the oxygen isotope composition of Korean speleothems remain unresolved. To interpret speleothem $\delta^{18}\text{O}$ records from the Korean Peninsula in detail, additional long-term high-resolution records and monitoring modern rainwater and cave water together with corresponding speleothems are needed.

5.4. Carbon isotopes

Six factors are generally thought to influence speleothem $\delta^{13}\text{C}$ values: (1) production of biogenic CO_2 by plant and soil processes, (2) relative ratio of C3 versus C4 plants, (3) soil-water residence time, (4) continued CO_2 degassing in the vadose zone, (5) contribution of limestone bedrock $\delta^{13}\text{C}$, and (6) isotopic composition of atmospheric CO_2 (Dorale et al., 1992; Baskaran and Krishnamurthy, 1993; Baker et al., 1997; Genty et al., 2003; Williams et al., 2004; Ford and Williams, 2007). In the present study, variations in C3/C4 plants and atmospheric $\delta^{13}\text{C}$ are unlikely to be important because C4 plants are not abundant in the mid-latitude, temperate Korean Peninsula (e.g., Cerling and Quade, 1993) and because even the maximum possible magnitude of atmospheric effects (change of less than 1‰ from the LGM to Holocene; Smith et al., 1999) is not sufficient to produce the $\delta^{13}\text{C}$ variations documented in DY-1 (about 4‰; Figs. 4 and 5). Any contribution of limestone $\delta^{13}\text{C}$ may

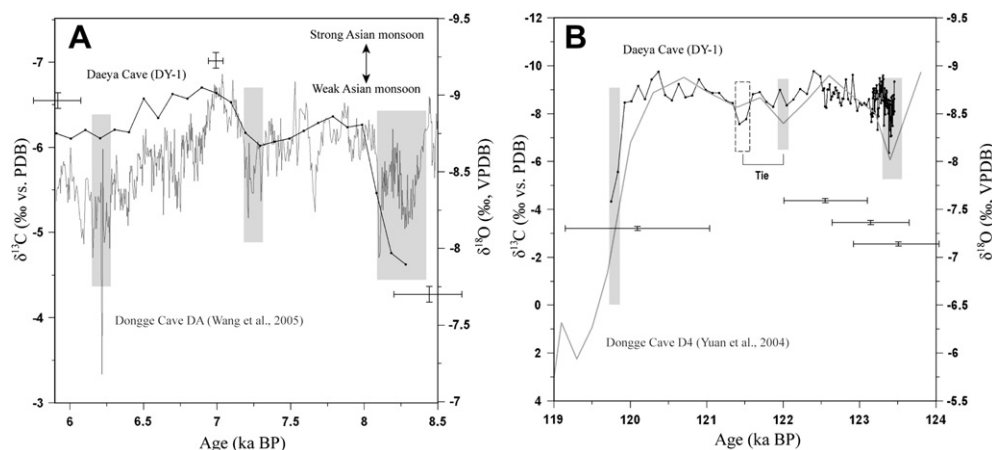


Fig. 5. $\delta^{13}\text{C}$ record of speleothem DY-1 (black line with dots) compared to $\delta^{18}\text{O}$ records from Dongge Cave (gray line, southern China; Yuan et al., 2004; Wang et al., 2005b). $\delta^{18}\text{O}$ and $\delta^{13}\text{C}$ values are plotted on the y-axis with values decreasing upwards. A) 8.5–5.7 ka. Gray bars represent Holocene weak monsoon events (Wang et al., 2005b). B) 124.0–119.0 ka. Gray bars indicate Eemian weak monsoon events and timing of the end of the Last Interglacial (Yuan et al., 2004). Analytical errors for carbon isotope compositions (0.2‰) and age dating are shown.

be negligible, based on the strontium geochemistry of a stalagmite from Songjia Cave in China (Zhou et al., 2008, 2009). Furthermore, results from a modern speleothem from the Korean Peninsula indicate that soil-water residence time, the effect of limestone $\delta^{13}\text{C}$, and continued degassing in the vadose zone are insignificant in DY-1 (Jo et al., 2010b). The obviously decreased $\delta^{13}\text{C}$ values in the modern speleothem during times of low rainfall are incompatible with the effects of limestone $\delta^{13}\text{C}$ and CO_2 degassing, both of which produce increased $\delta^{13}\text{C}$ values through longer water–rock interaction under cold, dry conditions. Soil-water residence time is irrelevant because the depleted $\delta^{13}\text{C}$ values that develop under dry climate conditions contrast with the results from DY-1 (Fig. 5). The differences between the modern precipitate and DY-1 can be explained by the formation of DY-1 over a much longer time span, during which significant vegetation changes took place, whereas the modern speleothem formed under constant vegetative conditions. In other words, seasonal or annual changes could have been embedded in centennial or millennial changes. If controlling factors responsible for long-term carbon isotope changes have influenced more on carbon isotope values of modern speleothems, other short-term variables should have been overwhelmed. Indeed, carbon isotope changes of only less than 1.5‰ were observed for the modern soda straw in Korea (Jo et al., 2010b), whereas long-term changes of carbon isotopes had exceeded more than 3–6‰. We thus concluded that, even though palaeoclimatic interpretation using carbon isotope compositions needs further scrutiny, variations in DY-1 $\delta^{13}\text{C}$ values appears to be primarily the result of variation in terrestrial palaeoproductivity such as vegetation respiration and/or related microbial activity (e.g., Hellstrom et al., 1998; Genty et al., 2003; Zhou et al., 2008).

Carbon isotopic compositions of DY-1 reflect East Asian monsoon changes recorded in Chinese Dongge Cave $\delta^{18}\text{O}$ records better than oxygen isotope values do (Fig. 5). This result agrees with previous results (Jo et al., 2010a) showing that although the $\delta^{18}\text{O}$ record from Gwaneum Cave (Fig. 1B) does not record general palaeoclimate changes of the Korean Peninsula, $\delta^{13}\text{C}$ exhibits higher values for cold, dry intervals and lower values for warm, wet intervals during MIS 5a, which concurs with $\delta^{18}\text{O}$ records of East Asian monsoon intensity from Chinese Sanbao Cave. This implies that variations in terrestrial palaeoproductivity in the Korean Peninsula have been directly affected by variations in East Asian monsoon intensity (Jo et al., 2010a), which are controlled by insolation changes (Wang et al., 2008).

6. Discussion

6.1. Growth history and palaeoclimatic implications

Experimental work has demonstrated that crystal morphology and growth mechanisms reflect the physicochemical conditions of the parent fluid (Sunagawa, 1987). In cave environments, speleothem calcite textures are controlled by environmental factors such as saturation state and discharge rate (González et al., 1992; Frisia et al., 2000). Although speleothem microstructures and their relationships with environmental conditions are not completely understood yet (Frisia et al., 2000), previous studies have successfully used speleothem calcite textures to interpret palaeoclimatic conditions (e.g., McDermott et al., 1999; Jo et al., 2010a). It is suggested here that the textures of DY-1 can be considered to be palaeoenvironmental indicators together with other analytical results and the age model, and they can also be used to interpret the growth history and palaeoclimatic conditions during the growth of DY-1.

Phases A and C in stalagmite DY-1 are entirely composed of large, fibrous to elongated columnar calcite crystals, indicating that

calcite precipitation took place at a low supersaturation state and under continuously wet conditions (Frisia et al., 2000; Figs. 2 and 3B). Such conditions would prevail during warm, wet interglacials or interstadials under the East Asian monsoon regime because stable hydrological conditions in the vadose zone require consistent precipitation and humidity (Jo et al., 2010a). In contrast, Phase B, which consists of mixtures of much smaller fibrous and micritic calcite crystals (corresponding to the tufa fabric described by Frisia et al., 2000) with frequent hiatus (Figs. 2 and 3C), is assumed to have formed under widely variable drip rates and/or episodic input of highly supersaturated cave drip-water under glacial or stadial conditions. These textural assumptions concur with the age model and isotopic results from DY-1.

During the middle of the Last Interglacial peak, optimal climatic conditions (high annual precipitation and high temperature; e.g., Khim et al., 2008; Wang et al., 2008) would have strongly affected the vegetation, epikarst, and vadose zone above Daeya Cave. During this time, the growth rate of Phase A reached its maximum owing to the large volumes of infiltrating rainwater, higher regional temperatures, and the higher partial pressure of CO_2 and concentration of Ca in drip waters (Dreybrodt, 1999; Fig. 2). The continuously warm, wet conditions were favorable to the uninterrupted growth of large, fibrous to elongated calcite crystals (Fig. 3A, B), at the same time as isotopic equilibrium was maintained between bicarbonate and CO_2 in the parent solution (Fig. 4B). These stable conditions persisted until 119.8 ka, with possible minor, gradual environmental changes since about 122.5 ka. A decreased growth rate but constant textural and carbon isotopic records in the upper part of Phase A suggest subtle environmental changes at that time (Figs. 2, 3A and 5B). Two explanations may be possible for this. Firstly, growth rate and $\delta^{13}\text{C}$ compositions were influenced by two different independent factors. In other words, carbon isotopic compositions could be controlled by local precipitation changes and growth rates by temperature changes. Secondly, even though both growth rate and $\delta^{13}\text{C}$ compositions were affected by local precipitation changes, the degree to which each of them was affected could have been quite different. It could well be possible that growth rate could be controlled by drip and degassing rates, temperature, and CO_3^{2-} concentrations of cave water (saturation state). It is not clear at present which factors were more effective for the DY-1 records and it needs further research. At 119.8 ka, the demise of the Last Interglacial East Asian monsoon significantly decreased the amount of precipitation and temperature in the Daeya Cave region (NGRIP members, 2004; Yuan et al., 2004). This overall climatic deterioration would have affected stalagmite DY-1 through episodicity of drip-water input, decreased cave temperature, and possibly greater cave ventilation, which are reflected in the extremely low growth rate, textural characteristics, and kinetic isotope fractionation of Phase B (Figs. 2, 3C, and 4B). These conditions were maintained until approximately 109.1 ka. Eventually, DY-1 stopped growing, probably due to very weak East Asian monsoon intensity and the inception of the last glacial (Fig. 2). DY-1 was unable to grow for the next 101 k.y., but growth resumed when the present interglacial peak was reached. From 8.6 to 5.9 ka, climatic conditions in the Daeya Cave area were recovered, although the improvement was not as pronounced as in the previous interglacial. DY-1 was once again influenced by continuously warm, wet conditions that produced both rapid, continuous growth of large, fibrous to elongated calcite crystals and isotopic equilibrium fractionation (Figs. 2, 3D, and 4B).

The growth history of DY-1 coincides with global climate changes as well as East Asian monsoon evolution (Berger, 1978; Martinson et al., 1987; Wang et al., 2001, 2008; NGRIP members, 2004; Yuan et al., 2004; Jouzel et al., 2007; Fig. 6). The temporal distribution of speleothem deposition has been used in South

Korea, England, Australia, Oman, and the Austrian Alps as an indicator of past times of warmer, wetter conditions (Baker et al., 1995; Ayliffe et al., 1998; Burns et al., 2001; Spötl et al., 2002; Jo et al., 2010a). These studies have shown good correlation between speleothem growth and periodic insolation maxima, pluvial events, marine isotope stratigraphy, and alpine glacier retreats. Two intervals of rapid growth in DY-1 can be correlated to the Holocene and Eemian climatic optima (e.g., Tzedakis, 2007).

The growth pattern and growth intervals of DY-1 are nearly identical to those of a Norwegian stalagmite that grew rapidly (46 mm/k.y.) between 123.4 and 119.5 ka, slowly (0.7 mm/k.y.) from 119.5 to 107.7 ka, and then again starting at 4.5 ka (Linge et al., 2001; Fig. 1A). The growth intervals of DY-1 are similar: Growth took place between 123.5 and 119.8 ka (Phase A; mean growth rate 20 mm/k.y.), between 119.8 and 109.1 ka (Phase B; 0.5 mm/k.y.), and from 8.6 ka to present (Phase C; Fig. 2). The growth history of DY-1 also concurs with the ^{230}Th dates of two significant eastern Mediterranean sapropel events (124.0–119.0 ka and 8.5–7.0 ka; Bar-Matthews et al., 2000; Fig. 6). Both rapid speleothem growth at the North Atlantic region and Mediterranean sapropel events are evident that climatic conditions at each region are particularly warm and/or wet. Numerous studies have noted the strong teleconnection between East Asian and North Atlantic regions, including the Mediterranean (e.g., Wang et al., 2001; Severinghaus, 2009; Jo et al., 2010a; Ziegler et al., 2010). For example, Severinghaus (2009) introduced that abrupt temperature decrease due to weakened North Atlantic deep water formation induced the southward migration of ITCZ (Intertropical Convergence Zone). Also, it is believed that this migration was directly related to weakened East Asian monsoon intensity. With related climates, similar speleothem growth patterns and stable isotope trends would be expected in the two regions.

6.2. Timing, duration, and evolution of Holocene and Eemian climatic optima

6.2.1. Holocene climatic optimum (HCO)

Comparison of the result in this study with other proxy records from Far East Asia indicates that the HCO in DY-1 may differ from established periods by about 1.5 ka. For example, pollen, mollusc-shell, coral, and peat records from South Korea, central to southern Japan, and southern to south-eastern China show that the Far East Asian sites experienced warmer, wetter conditions because of intensification of the East Asian monsoon between 10.0 and 4.5 ka (Yi et al., 2003a, 2003b, 2006; Schöne et al., 2004; Zhou et al., 2004; Morimoto et al., 2007; Yi and Kim, 2009). The timing and duration of the HCO in DY-1 coincide with well-dated stalagmite records from southern China and Oman. Intensification of Indian monsoon precipitation in southern Oman took place between 9.6 and 5.5 ka BP, according to stalagmite $\delta^{18}\text{O}$ values (Fleitmann et al., 2003; Fig. 1A), and $\delta^{18}\text{O}$ data from Dongge Cave (China) show a strong Asian monsoon interval from 9 to 7 ka, followed by a gradual weakening (Wang et al., 2005b; Figs. 1A and 7). The timing and duration of the HCO in DY-1 coincide with sapropel event 1 (9–6 ka) in the eastern Mediterranean (Rossignol-Strick, 1999; Bar-Matthews et al., 2000; Figs. 1A and 7) and ice-core records from northern Greenland (NGRIP members, 2004; Figs. 1A and 7). Even though the HCO interval in DY-1 is about 2.7 k.y. (8.6 ~ 5.9 ka) and is relatively shorter than Chinese speleothem records, these favorable comparisons suggest that the timing and duration of HCO in DY-1 are robust, and that the early to mid-HCO represents a general Holocene climatic amelioration, at least in the northern hemisphere.

An et al. (2000) and He et al. (2004) argued that the HCO in China initially affected higher altitudes in the north-west and only

gradually came to affect lower altitude locations in the south-east. In contrast, Zhou et al. (2004) suggested that the HCO in southern China was a regionally consistent event that took place between about 10 and 6 ka, which is consistent with the global pattern. Work on speleothems (Cai et al., 2010a) has found a pattern opposite to that proposed by An et al. (2000). Asynchrony of the HCO is difficult to demonstrate because Holocene climate change is of much lower amplitude than that of earlier interstadials.

As recorded in DY-1, the HCO began when insolation started to decrease from its maximum level, when temperature in Greenland was at a maximum, and when sea level reached its maximum level (Fig. 7). The HCO was, therefore, a product of the main climatic forcing factors: the balance among insolation, monsoon intensity, and sea level (=continental ice volume). For a climatic optimum to develop, all three of these controls had to have reached an inflection point in their respective cycles. If monsoon intensity, a direct function of insolation, was the main controlling factor behind the HCO, DY-1 should have grown during the other insolation maxima that took place between phases B and C (MISs 3, 5a, and 5b; Fig. 6). Maximum insolation leads to rapid continental ice melting, sea-level rise, and monsoon strengthening, whereas decreasing insolation would have caused the demise of the HCO. The timing of the HCO in the northern hemisphere is comparable to that of decreasing Antarctic temperature (Figs. 6 and 7), which may be explained by the bi-polar seesaw mechanism, in which Arctic and Antarctic temperatures vary antithetically (Stocker, 2000).

The DY-1 $\delta^{13}\text{C}$ record for the HCO displays weak monsoon events at 8.2, 7.2, and 6.1 ka with 1–2‰ fluctuations at millennial to centennial scales (Fig. 8). Such oscillations are also recorded in stalagmite $\delta^{18}\text{O}$ records from the East Asian and Indian monsoon regions (Figs. 1A and 8): records from Dongge (southern China) and Qunf (southern Oman) caves are clear (Fleitmann et al., 2003; Wang et al., 2005b), but the Sanbao $\delta^{18}\text{O}$ record (central China) is enigmatic (Wang et al., 2008). This correlation is possible based on two reasons. Firstly, overall trend between two records are similar and this trend is beyond the error range (Fig. 5). Secondly, carbon isotope values of the speleothem from other Korean cave (Jo et al., 2010a) show similar millennial-scale variations which are similar to the ones in Chinese speleothem records. Thus, it is very likely that similar changes in DY-1 may well reflect millennial-scale weak monsoon events in China. Holocene Asian monsoon intensity has been strongly affected by North Atlantic temperature variations, which are controlled by variations in solar output (Bond et al., 2001; Wang et al., 2005b). Abrupt climate changes caused by solar and meridional overturning circulation (MOC) effects probably could continue to affect the Far East Asian climate.

6.2.2. Eemian climatic optimum (ECO)

In contrast to the HCO, the timing and duration of the ECO are controversial (Muhs et al., 2002). The controversy arises presumably because of the variable sensitivities of different proxies and the lack of suitable age-determination methods. Although previous studies using direct or indirect dating methods have suggested that the ECO was achieved in Europe during the early- to mid-Eemian (129–125 ka; Björck et al., 2000; Brewer et al., 2008; Couchoud et al., 2009), the DY-1 record as well as a speleothem growth period from the Austrian Alps (Spötl et al., 2002) and a Bahamian sediment $\delta^{18}\text{O}$ record (Henderson and Slowey, 2000) indicate periods between about 123.0 and 118.0 ka for the ECO. Pollen, ice-core, and marine temperature records from the high-latitude North Atlantic and Mediterranean regions indicate that the European ECO peaked between 125 and 121 ka (Martrat et al., 2004; NGRIP members, 2004; Oppo et al., 2006; Tzedakis, 2007; Fig. 7). The DY-1 record is strongly supported by the growth pattern of a Norwegian speleothem (Linge et al., 2001) and the timing of

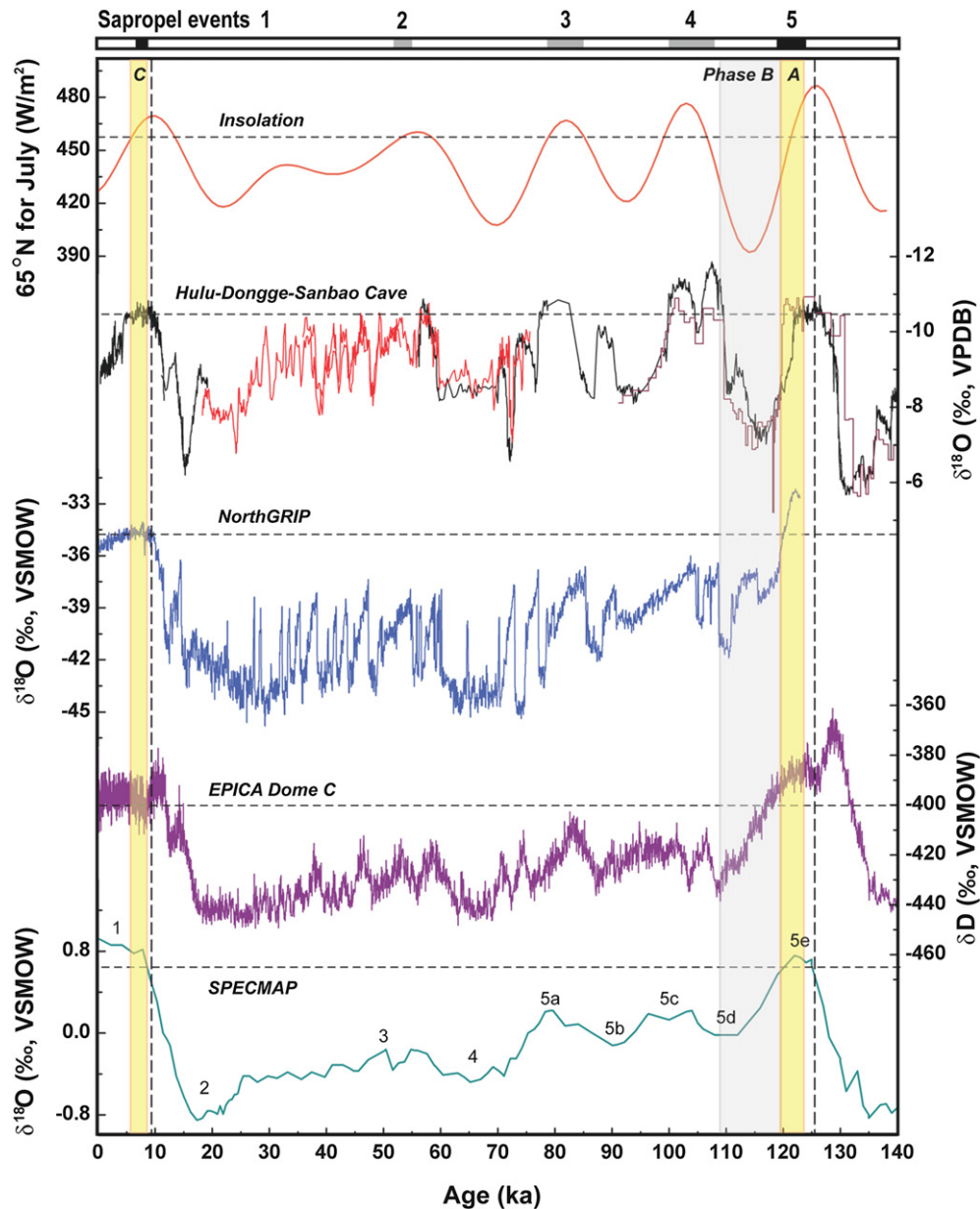


Fig. 6. Comparison of growth pattern from stalagmite DY-1 from the Korean Peninsula (yellow and light gray vertical bars) with long-term continuous palaeoclimatic records from other sites. Insolation at 65°N for July (orange; Berger, 1978), composite $\delta^{18}\text{O}$ records from Chinese caves (dark and light red and black; Wang et al., 2001, 2008; Yuan et al., 2004), northern Greenland and Antarctic ice-core $\delta^{18}\text{O}$ records (blue and purple; NGRIP members, 2004; Jouzel et al., 2007), and SPECMAP record (Martinson et al., 1987) are plotted. Eastern Mediterranean sapropel events (top) and insolation peak (vertical dashed lines) are also indicated for comparison. (For interpretation of the references to color in this figure legend, the reader is referred to the web version of this article.)

eastern Mediterranean sapropel event 5 (Bar-Matthews et al., 2000; Ziegler et al., 2010; Fig. 7). These similarities indicate that the first interval of rapid growth in DY-1 includes at least a large part of the ECO, and suggests that the ECO was reached in the Korean Peninsula shortly after 125 ka and lasted to around 120 ka, corresponding to the mid- to late-Eemian (Fig. 7).

ECO as well as HCO interval in DY-1 appears to be relatively shorter compared to other areas. However, evidence from stalagmite DY-1 is still supported by other records showing that the ECO commenced when insolation started to decrease from its maximum level, when temperature in Greenland was at its maximum, and when sea level had reached its maximum (Figs. 6 and 7). It is important to note that initiation of the ECO lagged behind the insolation maximum by about 2.2 k.y. Such a lag time is slightly different from that of the HCO (Fig. 7). However, HCO and

ECO records from DY-1 still suggest that both of the climatic optima in the Korean Peninsula may have been accomplished by similar causes and preconditions (Fig. 6). The Antarctic ice-core record shows that Holocene temperature decrease started 1.2 k.y. after the northern hemisphere insolation maximum, and Eemian temperature decrease began 0.7 k.y. prior to the insolation maximum (Fig. 7). These relationships may imply a complex relationship between Antarctic air temperature and northern hemisphere summer insolation (e.g., Cheng et al., 2006, 2009). Nevertheless, taken as a whole, the Antarctic ice-core record still permits correlation of the ECO interval in DY-1 with the temperature reversal that is centered at about 123.0 ka (Figs. 6 and 7), which would indicate activity of the bi-polar seesaw even during interglacial thermal maxima. Recently, Chylek et al. (2010) reported a bi-polar seesaw pattern in twentieth-century Arctic and Antarctic

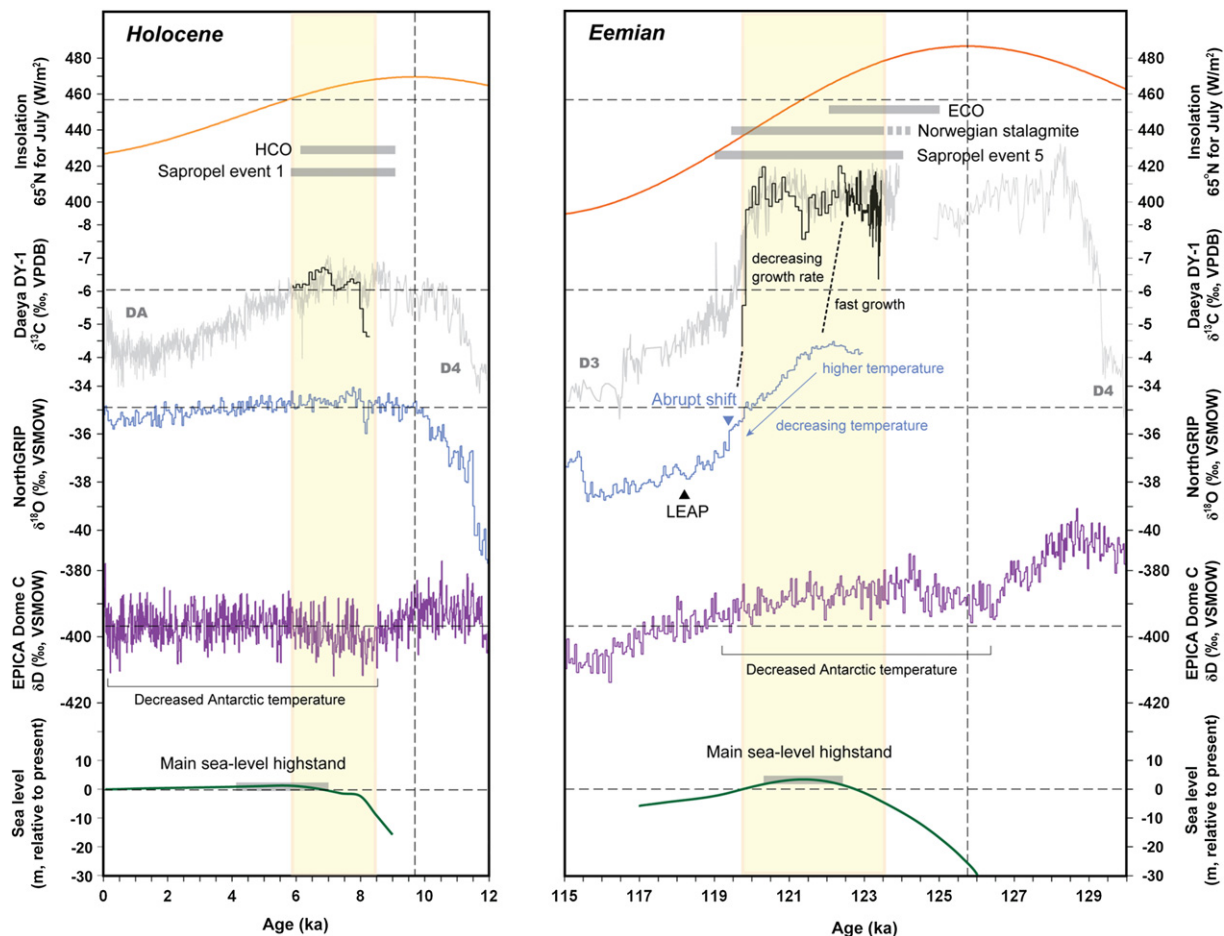


Fig. 7. Enlargement of Holocene and Eemian intervals from Fig. 6. The $\delta^{13}\text{C}$ record from DY-1 is shown. The DY-1 data are correlated with Chinese $\delta^{18}\text{O}$ records (DA, D3 and D4; light gray) without their scales to trace changes of Asian monsoon climate (Wang et al., 2005b; Dykoski et al., 2005; Kelly et al., 2006). D3 data are presented using the better time scale of Yuan et al. (2004). Time intervals of Holocene (Wang et al., 2005b) and Eemian (Oppo et al., 2006) climatic optima, main sea-level highstands (ca more 2 m higher than present sea level for HCO, Bird et al., 2010; ca more 5 m higher than present for ECO, Rohling et al., 2008), rapid growth interval of a Norwegian stalagmite (Linge et al., 2001), and speleothem-based Mediterranean sapropel events (Rossignol-Strick, 1999; Bar-Matthews et al., 2000) are also shown. Black triangle represents the late Eemian aridity pulse (LEAP; Sirocko et al., 2005). Blue inverted triangle indicates a relatively abrupt shift in NGRIP $\delta^{18}\text{O}$ values. (For interpretation of the references to color in this figure legend, the reader is referred to the web version of this article.)

temperature records. This finding highlights the possibility that climatic optimal records for past interglacials can serve as ancient counterparts for current and future warming, even though their orbital and anthropogenic forcing factors are largely different. It also introduces the possibility of age-tuning past interglacial climatic optima for indirectly dated proxy records.

The Eemian $\delta^{13}\text{C}$ record of DY-1 is characterized by an abrupt shift of about 4‰ at 119.8 ka and two positive anomalies of more than 1‰ at 121.4 and 123.4 ka (Fig. 8). Although Eemian millennial-scale fluctuations from East Asia have not yet been proposed, these shifts are similar to the Chinese Dongge $\delta^{18}\text{O}$ records (Yuan et al., 2004; Kelly et al., 2006; Fig. 8). Millennial-scale climate variability has been recorded in stalagmite, lake-sediment, and pollen records from northern and central Europe (Björck et al., 2000; Müller et al., 2005; Couchoud et al., 2009). Biogenic silica records from Lake Baikal in central Asia provide evidence of mid-Eemian cooling (Karabanov et al., 2000, and references therein). Despite the uncertainties of the exact timing of such events, $\delta^{13}\text{C}$ results of the present study indicate that the ECO recorded in DY-1 generally follow other global trend. According to previous studies (Bond et al., 2001; Müller et al., 2005), Eemian climate variability may have been caused by changes in solar activity, possibly amplified by

changes in North Atlantic ocean currents and/or in the North Atlantic Oscillation. In DY-1, the faster growth rate and lower $\delta^{13}\text{C}$ values of Phase A (relative to those of Phase C) indicate that Eemian climatic conditions were warmer than those of the Holocene. This difference can be also deduced by the difference in sea level, because it is generally well known that the sea level during the Eemian period was higher than during the Holocene by a few meters (e.g., Rohling et al., 2008).

The large shift in $\delta^{13}\text{C}$ values in DY-1 at 119.8 ka represents the demise of the Last Interglacial Asian monsoon. This carbon isotopic signal is in agreement with stalagmite $\delta^{18}\text{O}$ records from southern to central China and the Himalayan region (Yuan et al., 2004; Kelly et al., 2006; Wang et al., 2008; Cai et al., 2010b; Fig. 8). The demise of the Last Interglacial Asian monsoon was simultaneous in disparate areas within the error range. DY-1 and Dongge records are in particularly good agreement, whereas Himalayan data suggest an earlier inception than elsewhere. The possibility of asynchrony in the demise of the Last Interglacial Asian monsoon requires further research. Within the error range, the demise of the Last Interglacial in the DY-1 record coincides with a large shift in the speleothem $\delta^{18}\text{O}$ record from the eastern Mediterranean (Bar-Matthews et al., 2000), the relatively abrupt shift in the

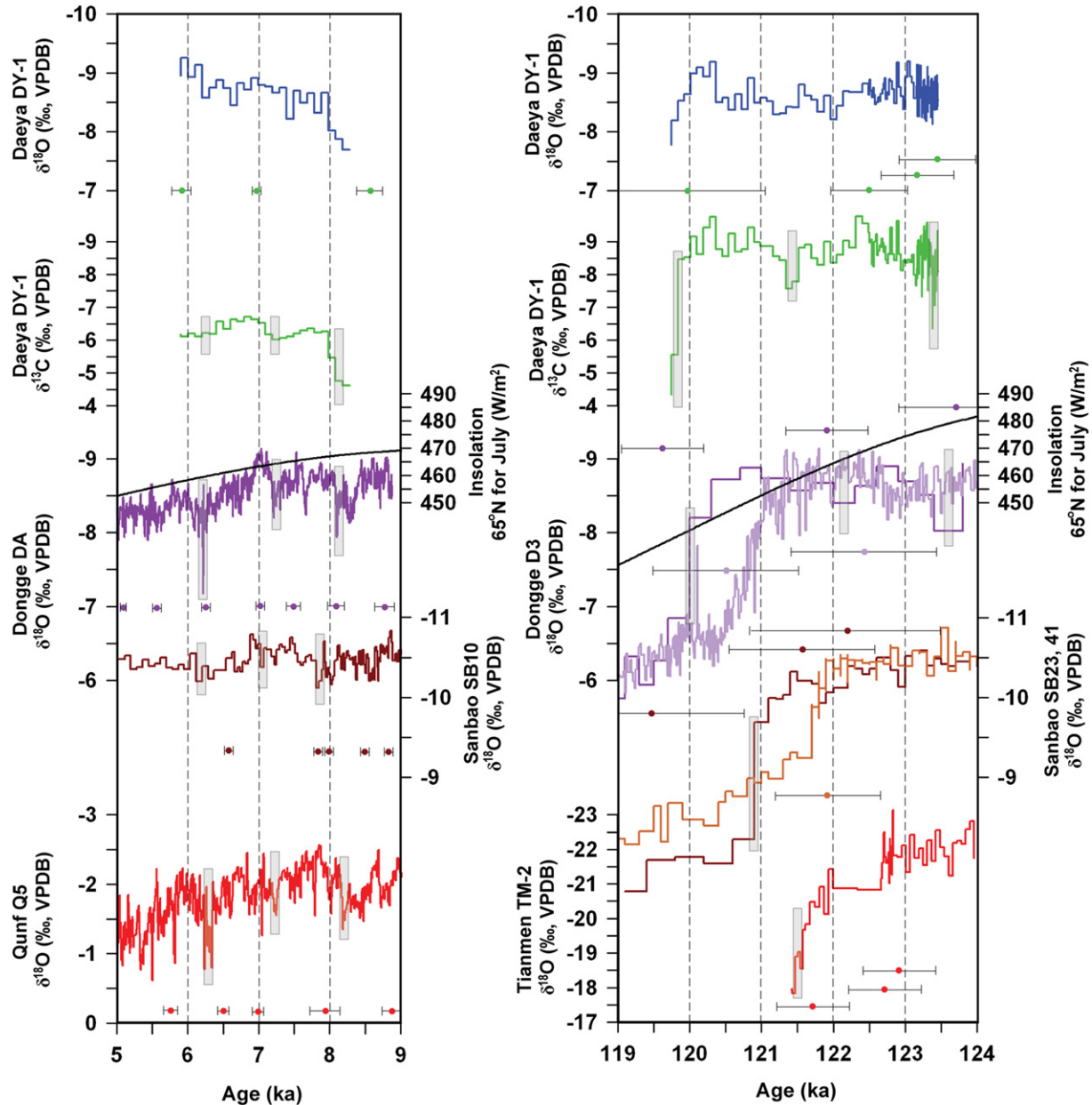


Fig. 8. Comparison of $\delta^{18}\text{O}$ (blue) and $\delta^{13}\text{C}$ (green) records from DY-1 with stalagmite $\delta^{18}\text{O}$ records from Dongge Cave (China; dark and light purple; Yuan et al., 2004; Wang et al., 2005b; Kelly et al., 2006), Sanbao Cave (China; dark and light brown; Wang et al., 2008), Tianmen Cave (Tibet; red; Cai et al., 2010b), and Qunf Cave (Oman; red; Fleitmann et al., 2003). All records are shown with 2σ error ranges. Age dating results are shown with colored dots with error bars. Also shown are millennial-scale weak monsoon events (gray bars). Note the positive anomalies at 121.4 and 123.4 ka for Eemian record. The English in this document has been checked by at least two professional editors, both native speakers of English. For a certificate, please see: <http://www.textcheck.com/certificate/9CT8OS>. (For interpretation of the references to color in this figure legend, the reader is referred to the web version of this article.)

NorthGRIP ice-core $\delta^{18}\text{O}$ record (NGRIP members, 2004), and the late Eemian aridity pulse (LEAP) recorded in maar lake sediment of Eifel (Germany; Sirocko et al., 2005; Fig. 7). This may suggest the contemporaneous onset of glaciation in the North Atlantic, Mediterranean, and Asian regions.

7. Summary

This paper presents a palaeo-monsoonal record from stalagmite DY-1 from the Korean Peninsula for the Holocene and Eemian climatic optima. Well-developed fibrous to elongated columnar calcite, depleted carbon isotopic compositions, and faster growth rates of the stalagmite reflect the warmest and wettest

palaeoclimates, which were caused by intensified East Asian monsoons during the Holocene and Eemian interglacials. Both intervals of climatic optimum conditions in the Korean Peninsula began at the same time as insolation started to decrease from its maximum level, Greenlandic temperature reached its maximum, and sea level reached its maximum level. Northern hemispheric climatic optima can be correlated with the timing of decreasing Antarctic temperature. These trends also follow the bi-polar seesaw mechanism as previously described. The $\delta^{13}\text{C}$ record of DY-1 also implies that even optimal interglacial conditions are variable and include millennial-scale variability that is presumably caused by changes in solar activity, and possibly amplified by changes in North Atlantic Ocean circulation and/or in the North Atlantic Oscillation.

Acknowledgments

This work was supported by the K-Polar Program (PP11010) of the Korea Polar Research Institute and the Korea Meteorological Administration Research and Development Program (RACS 2010-3007, PN10040). This research was also supported in part by the project of the research on the abrupt climate change for the prediction of extreme geo-hazards and sea level change around the Korean Peninsula (GP2009-005) funded by the Korea Institute of Geoscience and Mineral Resources (KIGAM). We thank the person in charge of natural heritages in Yeongweol-gun, Gangwon-do, South Korea for authorizing cave sample collection and KNUCIC (Kangwon National University Cave Investigation Club) members for supporting field work. First author thanks for financial support from the post-doctoral research program of Kangwon National University. The authors are grateful to the Dr. Hillaire-Marcel, Dr. Huang, and two anonymous reviewers for helpful reviews and suggestions.

Appendix. Supplementary data

Supplementary data related to this article can be found online at doi:10.1016/j.quascirev.2011.02.012.

References

- An, Z., Porter, S.C., Kutzbach, J.E., Xihao, W., Suming, W., Xiaodong, L., Xiaoqiang, L., Weijian, Z., 2000. Asynchronous Holocene optimum of the east Asian monsoon. *Quaternary Science Reviews* 19, 743–762.
- Anderson, T.F., Arthur, M.A., 1983. Stable isotopes of oxygen and carbon and their application to sedimentologic and paleoenvironmental problems. In: Arthur, M.A., Anderson, T.F., Kaplan, I.R., Veizer, J. (Eds.), *Stable Isotopes in Sedimentary Geology*, pp. 1–151. SEPM Short Course No. 10.
- Asmerom, Y., Polyak, V., Burns, S., Rasmussen, J., 2007. Solar forcing of Holocene climate: new insights from a speleothem record, southwestern United States. *Geology* 35, 1–4.
- Ayliffe, L.K., Marianelli, P.C., Moriarty, K.C., Wells, R.T., McCulloch, M.T., Mortimer, G.E., Hellstrom, J.C., 1998. 500 ka precipitation record from south-eastern Australia: evidence for interglacial relative aridity. *Geology* 26, 147–150.
- Baker, A., Smart, P.L., Edwards, R.L., 1995. Paleoclimate implications of mass spectrometric dating of a British flowstone. *Geology* 23, 309–312.
- Baker, A., Ito, E., Smart, P.L., McEwan, R.F., 1997. Elevated and variable values of $\delta^{13}\text{C}$ in speleothems in a British cave system. *Chemical Geology* 136, 263–270.
- Bar-Matthews, M., Ayalon, A., Kaufman, A., 2000. Timing and hydrological conditions of Sapropel events in the Eastern Mediterranean, as evident from speleothems, Soreq cave, Israel. *Chemical Geology* 169, 145–156.
- Baskaran, M., Krishnamurthy, R.V., 1993. Speleothems as proxy for the carbon isotope composition of atmospheric CO_2 . *Geophysical Research Letters* 20, 2905–2908.
- Berger, A.L., 1978. Long-term variations of caloric insolation resulting from the Earth's orbital elements. *Quaternary Research* 9, 139–167.
- Bird, M.I., Austin, W.E.N., Wurster, C.M., Fifield, L.K., Mojtabid, M., Sargeant, C., 2010. Punctuated eustatic sea-level rise in the early mid-Holocene. *Geology* 38, 803–806.
- Björck, S., Noe-Nygaard, N., Wolin, J., Houmark-Nielsen, M., Hansen, H.J., Snowball, I., 2000. Eemian Lake development, hydrology and climate: a multi-stratigraphic study of the Hollerup site in Denmark. *Quaternary Science Reviews* 19, 509–536.
- Brewer, S., Guiot, J., Sánchez-Goñi, M.F., Klotz, S., 2008. The climate in Europe during the Eemian: a multi-method approach using pollen data. *Quaternary Science Reviews* 27, 2303–2315.
- Boch, R., Spötl, C., Kramers, J., 2009. High-resolution isotope records of early Holocene rapid climate change from two coeval stalagmites of Katerloch Cave, Austria. *Quaternary Science Reviews* 28, 2527–2538.
- Bond, G., Kromer, B., Beer, J., Muscheler, R., Evans, M.N., Showers, W., Hoffmann, S., Lotti-Bond, R., Hajdas, I., Bonani, G., 2001. Persistent solar influence on North Atlantic climate during the Holocene. *Science* 294, 2130–2136.
- Burns, S.J., Fleitmann, D., Matter, A., Neff, U., Mangini, A., 2001. Speleothem evidence from Oman for continental pluvial events during interglacial periods. *Geology* 29, 623–626.
- Cai, Y., Cheng, H., An, Z., Edwards, R.L., Wang, X., Tan, L., Wang, J., 2010a. Large variations of oxygen isotopes in precipitation over south-central Tibet during Marine Isotope Stage 5. *Geology* 38, 243–246.
- Cai, Y., Tan, L., Cheng, H., An, Z., Edwards, R.L., Kelly, M.J., Kong, X., Wang, X., 2010b. The variation of summer monsoon precipitation in central China since the last deglaciation. *Earth and Planetary Science Letters* 291, 21–31.
- Cerling, T.E., Quade, J., 1993. Stable carbon and oxygen isotopes in soil carbonates. In: Swart, P.K., Lohmann, K.C., McKenzie, J., Savin, S. (Eds.), *Climate Change in Continental Isotopic Records*. American Geophysical Union, Washington, DC, pp. 217–231.
- Cheng, H., Edwards, R.L., Wang, Y., Kong, X., Ming, Y., Kelly, M.J., Wang, X., Gallup, C.D., Liu, W., 2006. A penultimate glacial monsoon record from Hulu Cave and two-phase glacial terminations. *Geology* 34, 217–220.
- Cheng, H., Edwards, R.L., Broecker, W.S., Denton, G.H., Kong, X., Wang, Y., Zhang, R., Wang, X., 2009. Ice age terminations. *Science* 326, 248–252.
- Chough, S.K., Kwon, S.-T., Ree, J.-H., Choi, D.K., 2000. Tectonic and sedimentary evolution of the Korean peninsula: a review and new view. *Earth-Science Reviews* 52, 175–235.
- Chylek, P., Folland, C.K., Lesins, G., Dubey, M.K., 2010. Twentieth century bipolar seesaw of the Arctic and Antarctic surface air temperatures. *Geophysical Research Letters* 37, L08703.
- Cosford, J., Qing, H., Eglinton, B., Matthey, D., Yuan, D., Zhang, M., Cheng, H., 2008. East Asian monsoon variability since the Mid-Holocene recorded in a high-resolution, absolute-dated aragonite speleothem from eastern China. *Earth and Planetary Science Letters* 275, 296–307.
- Cosford, J., Qing, H., Lin, Y., Eglinton, B., Matthey, D., Chen, Y.G., Zhang, M., Cheng, H., 2010. The east Asian monsoon during MIS 2 expressed in a speleothem $\delta^{18}\text{O}$ record from Jintanwan cave, Hunan, China. *Quaternary Research* 73, 541–549.
- Couchoud, I., Genty, D., Hoffmann, D., Drysdale, R., Blamart, D., 2009. Millennial-scale climate variability during the Last Interglacial recorded in a speleothem from south-western France. *Quaternary Science Reviews* 28, 3263–3274.
- Dorale, J.A., González, L.A., Reagan, M.K., Pickett, D.A., Murrell, M.T., Baker, R.G., 1992. A high-resolution record of Holocene climate change in speleothem calcite from Cold Water Cave, Northeast Iowa. *Science* 258, 1626–1630.
- Dorale, J.A., Liu, Z., 2009. Limitations of Hendy Test criteria in judging the paleoclimatic suitability of speleothems and the need for replication. *Journal of Cave and Karst Studies* 71, 73–80.
- Dreybrodt, W., 1999. Chemical kinetics, speleothem growth and climate. *Boreas* 28, 347–356.
- Drysdale, R.N., Zanchetta, G., Hellstrom, J.C., Fallick, A.E., Zhao, J.-x., 2005. Stalagmite evidence for the onset of the Last Interglacial in southern Europe at 129 ± 1 ka. *Geophysical Research Letters* 32, L24708.
- Dykoski, C.A., Edwards, R.L., Cheng, H., Yuan, D., Cai, Y., Zhang, M., Lin, Y., Qing, J., An, Z., Revenaugh, J., 2005. A high-resolution, absolute-dated Holocene and deglacial Asian monsoon record from Dongge Cave, China. *Earth and Planetary Science Letters* 233, 71–86.
- Fleitmann, D., Spötl, C., 2008. Advances in speleothem research. *PAGES news*, 16, 2.
- Fleitmann, D., Burns, S.J., Mudelsee, M., Neff, U., Kramers, J., Mangini, A., Matter, A., 2003. Holocene forcing of the Indian monsoon recorded in a stalagmite from Southern Oman. *Science* 300, 1737–1739.
- Ford, D., Williams, P., 2007. *Karst Hydrogeology and Geomorphology*. John Wiley & Sons, Ltd., West Sussex, pp. 306–320.
- Frisia, S., Borsato, A., Fairchild, I.J., McDermott, F., 2000. Calcite fabrics, growth mechanisms, and environments of formation in speleothems from the Italian Alps and southwestern Ireland. *Journal of Sedimentary Research* 70, 1183–1196.
- Gascoyne, M., Schwarcz, H.P., Ford, D.C., 1980. A palaeotemperature record for the mid-Wisconsin in Vancouver Island. *Nature* 285, 474–476.
- Genty, D., Blamart, D., Ouahdi, R., Gilmour, M., Baker, A., Jouzel, J., Van-Exter, S., 2003. Precise dating of Dansgaard-Oeschger climate oscillations in western Europe from stalagmite data. *Nature* 421, 833–837.
- González, L.A., Carpenter, S.J., Lohmann, K.C., 1992. Inorganic calcite morphology: roles of fluid chemistry and fluid flow. *Journal of Sedimentary Petrology* 62, 382–399.
- He, Y., Theakstone, W.H., Zhonglin, Z., Dian, Z., Tandong, Y., Tuo, C., Yongping, S., Hongxi, P., 2004. Asynchronous Holocene climatic change across China. *Quaternary Research* 61, 52–63.
- Hellstrom, J., McCulloch, M., Stone, J., 1998. A detailed 31,000-year record of climate and vegetation change, from the isotope geochemistry of two New Zealand speleothems. *Quaternary Research* 50, 167–178.
- Henderson, G.M., Slowey, N.C., 2000. Evidence from U-Th dating against Northern Hemisphere forcing of the penultimate deglaciation. *Nature* 404, 61–66.
- Hendy, C., 1971. The isotopic geochemistry of speleothems-I. The calculation of the effects of different modes of formation on the isotopic composition of speleothems and their applicability as paleoclimatic indicators. *Geochimica et Cosmochimica Acta* 35, 801–824.
- IPCC, 2007. *Climate change 2007: the physical science basis. Contribution of working Group I to the Fourth Assessment report of the Intergovernmental panel on climate change*. In: Solomon, S., Qin, D., Manning, M., Chen, Z., Marquis, M., Averyt, K.B., Tignor, M., Miller, H.L. (Eds.), *Climate change 2007: the physical science basis. Contribution of working Group I to the Fourth Assessment report of the Intergovernmental panel on climate change*. Cambridge University Press, Cambridge, United Kingdom and New York, NY, USA.
- Jo, K., Woo, K.S., Cheng, H., Edwards, R.L., Wang, Y., Kim, R., Jiang, X., 2010a. Textural and carbon isotopic evidence of monsoonal changes recorded in a composite-type speleothem from Korea since MIS 5a. *Quaternary Research* 74, 100–112.
- Jo, K., Woo, K.S., Hong, G.H., Kim, S.H., Suk, B.C., 2010b. Rainfall and hydrological controls on speleothem geochemistry during climatic events (droughts and typhoons): an example from Seodong Cave, Republic of Korea. *Earth and Planetary Science Letters* 295, 441–450.

- Jouzel, J., Masson-Delmotte, V., Cattani, O., Dreyfus, G., Falourd, S., Hoffmann, G., Minster, B., Nouet, J., Barnola, J.M., Chappellaz, J., Fischer, H., Gallet, J.C., Johnsen, S., Leuenberger, M., Loulergue, L., Luethi, D., Oerter, H., Parrenin, F., Raisbeck, G., Raynaud, D., Schilt, A., Schwander, J., Selmo, E., Souchez, R., Spahni, R., Stauffer, B., Steffensen, J.P., Stenni, B., Stocker, T.F., Tison, J.L., Werner, M., Wolff, E.W., 2007. Orbital and millennial Antarctic climate variability over the past 8,000,000 years. *Science* 317, 793–796.
- Karabanov, E.B., Prokopenko, A.A., Williams, D.F., Khursevich, G.K., 2000. Evidence for mid-Eemian cooling in continental climatic record from Lake Baikal. *Journal of Paleolimnology* 23, 365–371.
- Kelly, M.J., Edwards, R.L., Cheng, H., Yuan, D., Cai, Y., Zhang, M., Lin, Y., An, Z., 2006. High-resolution characterization of the Asian Monsoon between 1,46,000 and 99,000 years B.P. from Dongge Cave, China and global correlation of events surrounding Termination II. *Palaeogeography, Palaeoclimatology, Palaeoecology* 326, 20–38.
- Khim, B.K., Park, Y.H., Bahk, J.J., Jin, J.H., Lee, G.H., 2008. Spatial and temporal variation of geochemical properties and paleoceanographic implications in the South Korea Plateau (East Sea) during the late Quaternary. *Quaternary International* 176–177, 46–61.
- Kukla, G., Bender, M.L., de Beaulieu, J.-L., Bond, G., Broecker, W.S., Clevinger, P., Gavin, J.E., Herbert, T.D., Imbrie, J., Jouzel, J., Keigwin, L.D., Knudsen, K.-L., McManus, J.F., Merkt, J., Muhs, D.R., Müller, H., Poore, R.Z., Porter, S.C., Seret, G., Shackleton, N.J., Turner, C., Tzedakis, P.C., Winograd, I.J., 2002. Last interglacial climates. *Quaternary Research* 58, 2–13.
- Lee, K.E., 2007. Surface water changes recorded in late Quaternary marine sediments of the Ulleung Basin, East Sea (Japan Sea). *Palaeogeography, Palaeoclimatology, Palaeoecology* 247, 18–31.
- Lee, J.-E., Johnson, K., Fung, I., 2009. Precipitation over South America during the Last Glacial Maximum: an analysis of the “amount effect” with a water isotope-enabled general circulation model. *Geophysical Research Letters* 36, L19701.
- Linge, H., Lauritzen, S.-E., Lundberg, J., 2001. Stable isotope stratigraphy of a late Last Interglacial speleothem from Rana, northern Norway. *Quaternary Research* 56, 155–164.
- Martinson, D.G., Pisias, N.G., Hays, J.D., Imbrie, J., Moore, T.C., Shackleton, N.J., 1987. Age dating and the orbital theory of the ice ages: development of a high-resolution 0 to 3,00,000-year chronostratigraphy. *Quaternary Research* 27, 1–29.
- Martrat, B., Grimalt, J.O., Lopez-Martinez, C., Cacho, I., Sierro, F.J., Flores, J.A., Zahn, R., Canals, M., Curtis, J.H., Hodell, D.A., 2004. Abrupt temperature changes in the western Mediterranean over the past 2,500,000 years. *Science* 306, 1762–1765.
- McDermott, F., Frisia, S., Huang, Y., Longinelli, A., Spiro, B., Heaton, T.H.E., Hawkesworth, C.J., Borsato, A., Keppens, E., Fairchild, I.J., Borg, K., Verheyden, S., Selmo, E., 1999. Holocene climate variability in Europe: evidence from $\delta^{18}\text{O}$, textural and extension-rate variations in three speleothems. *Quaternary Science Reviews* 18, 1021–1038.
- Morimoto, M., Kayanne, H., Abe, O., McCulloch, M.T., 2007. Intensified mid-Holocene Asian monsoon recorded in corals from Kikai Island, subtropical north-western Pacific. *Quaternary Research* 67, 204–214.
- Muhs, D.R., Simmons, K.R., Steinke, B., 2002. Timing and warmth of the Last Interglacial period: new U-series evidence from Hawaii and Bermuda and a new fossil compilation for North America. *Quaternary Science Reviews* 21, 1355–1383.
- Müller, U.C., Klotz, S., Geyh, M.A., Pross, J., Bond, G.C., 2005. Cyclic climate fluctuations during the Last Interglacial in central Europe. *Geology* 33, 449–452.
- NGRIP (North Greenland Ice Core Project) members, 2004. High-resolution record of Northern Hemisphere climate extending into the Last Interglacial period. *Nature* 431, 147–151.
- Oppo, D.W., McManus, J.F., Cullen, J.L., 2006. Evolution and demise of the Last Interglacial warmth in the subpolar north Atlantic. *Quaternary Science Reviews* 25, 3268–3277.
- Rohling, E.J., Grant, K., Hemleben, C.H., Siddall, M., Hoogakker, B.A.A., Bolshaw, M., Kucera, M., 2008. High rates of sea-level rise during the Last Interglacial period. *Nature Geoscience* 1, 38–42.
- Rosignol-Strick, M., 1999. The Holocene climatic optimum and pollen records of sapropel 1 in the eastern Mediterranean, 9000–6000 BP. *Quaternary Science Reviews* 18, 515–530.
- Schöne, B.R., Oschmann, W., Tanabe, K., Dettman, D., Fiebig, J., Houk, S.D., Kanie, Y., 2004. Holocene seasonal environmental trends at Tokyo Bay, Japan, reconstructed from bivalve mollusk shells—implications for changes in the East Asian monsoon and latitudinal shifts of the Polar Front. *Quaternary Science Reviews* 23, 1137–1150.
- Severinghaus, J.P., 2009. Monsoons and melt-downs. *Science* 326, 240–241.
- Shackleton, N.J., Sánchez-Goni, M.F., Pailler, D., Lancelot, Y., 2003. Marine Isotope Substage 5e and the Eemian Interglacial. *Global and Planetary Change* 36, 151–155.
- Sirocko, F., Seelos, K., Schaber, K., Rein, B., Dreher, F., Diehl, M., Lehne, R., Jäger, K., Krbetschek, M., Degering, D., 2005. A late Eemian aridity pulse in central Europe during the last glacial inception. *Nature* 436, 833–836.
- Smith, H.J., Fischer, H., Wahlen, M., Mastroianni, D., Deck, B., 1999. Dual modes of the carbon cycle since the Last Glacial Maximum. *Nature* 400, 248–250.
- Spötl, C., Mangini, A., Frank, N., Eichstädter, R., Burns, S.J., 2002. Start of the Last Interglacial period at 135 ka: evidence from a high Alpine speleothem. *Geology* 30, 815–818.
- Stocker, T.F., 2000. Past and future reorganizations in the climate system. *Quaternary Science Reviews* 19, 301–319.
- Sunagawa, I., 1987. Morphology of minerals. In: Sunagawa, I. (Ed.), *Morphology of Crystals*. Terra Scientific Publishing Company, Tokyo, pp. 509–587.
- Tzedakis, C., 2007. Pollen records, Last Interglacial of Europe. In: Elia, S.A. (Ed.), *Encyclopedia of Quaternary Science*, Vol. 4, pp. 2597–2605.
- Wang, P., Clemens, S., Beaufort, L., Braconnot, P., Ganssen, G., Jian, Z., Kershaw, P., Sarntheim, M., 2005a. Evolution and variability of the Asian monsoon system: state of the art and outstanding issues. *Quaternary Science Reviews* 24, 595–629.
- Wang, Y.J., Cheng, H., Edwards, R.L., An, Z.S., Wu, J.Y., Shen, C.-C., Dorale, J.A., 2001. A high-resolution absolute-dated late Pleistocene monsoon record from Hulu Cave, China. *Science* 294, 2345–2348.
- Wang, Y., Cheng, H., Edwards, R.L., He, Y., Kong, X., An, Z., Wu, J., Kelly, M.J., Dykoski, C.A., Li, X., 2005b. The Holocene Asian monsoon: links to solar changes and North Atlantic Climate. *Science* 308, 854–857.
- Wang, Y., Cheng, H., Edwards, R.L., Kong, X., Shao, X., Chen, S., Wu, J., Jiang, X., Wang, X., An, Z., 2008. Millennial- and orbital-scale changes in the East Asian monsoon over the past 2,24,000 years. *Nature* 451, 1090–1093.
- Wanner, H., Beer, J., Büttikofer, J., Crowley, T.J., Cubasch, U., Flückiger, J., Goosse, H., Grosjean, M., Joos, F., Kaplan, J.O., Küttel, M., Müller, S.A., Prentice, I.C., Solomina, O., Stocker, T.F., Tarasov, P., Wagner, M., Widmann, M., 2008. Mid- to Late Holocene climate change: an overview. *Quaternary Science Reviews* 27, 1791–1828.
- Williams, P.W., King, D.N.T., Zhao, J.-X., Collerson, K.D., 2004. Speleothem master chronologies: combined Holocene $\delta^{18}\text{O}$ and $\delta^{13}\text{C}$ records from the North Island of New Zealand and their palaeo-environmental interpretation. *The Holocene* 14, 194–208.
- Woo, K.S., Park, B.K., 1989. Depositional environments and diagenesis of the sedimentary rocks, Choseon Supergroup, Korea: past, present, and future; the state of the art. *Journal of the Geological Society of Korea* 25, 347–363.
- Yi, S., Saito, Y., Oshima, H., Zhou, Y., Wei, H., 2003a. Holocene environmental history inferred from pollen assemblages in the Huanghe (Yellow River) delta, China: climatic change and human impact. *Quaternary Science Reviews* 22, 609–628.
- Yi, S., Saito, Y., Zhao, Q., Wang, P., 2003b. Vegetation and climate changes in the Changjiang (Yangtze River) Delta, China, during the past 13,000 years inferred from pollen records. *Quaternary Science Reviews* 22, 1501–1519.
- Yi, S., Saito, Y., Yang, D.-Y., 2006. Palynological evidence for Holocene environmental change in the Changjiang (Yangtze River) delta, China. *Paleogeography, Palaeoclimatology, Palaeoecology* 241, 103–117.
- Yi, S., Kim, J.-Y., 2009. Pollen indication of Holocene vegetation and environments in the Sacheon-dong archaeological site, Cheongju, Chungbuk province (In Korean with English abstract). *Journal of Paleontological Society of Korea* 25, 63–76.
- Yu, J.-Y., Park, Y., Mielke, R.E., Coleman, M.L., 2007. Sulfur and oxygen isotopic compositions of the dissolved sulphate in the meteoric water in Chuncheon, Korea. *Geosciences Journal* 11, 357–367.
- Yuan, D., Cheng, H., Edwards, R.L., Dykoski, C.A., Kelly, M.J., Zhang, M., Qing, J., Lin, Y., Wang, Y., Wu, J., Dorale, J.A., An, Z., Cai, Y., 2004. Timing, duration, and Transitions of the Last Interglacial Asian monsoon. *Science* 304, 575–578.
- Zhou, W., Yu, X., Jull, A.J.T., Burr, G., Xiao, J.Y., Lu, X., Xian, F., 2004. High-resolution evidence from southern China of an early Holocene optimum and a mid-Holocene dry event during the past 18,000 years. *Quaternary Research* 62, 39–48.
- Zhou, H., Zhao, J., Feng, Y., Gagan, M.K., Zhou, G., Yan, J., 2008. Distinct climate change synchronous with Heinrich event one, recorded by stable oxygen and carbon isotopic compositions in stalagmites from China. *Quaternary Research* 69, 306–315.
- Zhou, H., Feng, Y., Zhao, J., Shen, C.-C., You, C.-F., Lin, Y., 2009. Deglacial variations of Sr and $^{87}\text{Sr}/^{86}\text{Sr}$ ratio recorded by a stalagmite from Central China and their association with past climate and environment. *Chemical Geology* 268, 233–247.
- Ziegler, M., Tuenter, E., Lourens, L.J., 2010. The precession phase of the boreal summer monsoon as viewed from the eastern Mediterranean (ODP Site 968). *Quaternary Science Reviews* 29, 1481–1490.